

1 An updated synthesis of ocean total alkalinity and dissolved inorganic carbon measurements
2 from 1993 to 2023: the SNAPO-CO2-v2 dataset

3
4 Nicolas Metzl¹, Jonathan Fin^{1,2,3}, Claire Lo Monaco¹, Claude Mignon¹, Samir Alliouane⁴, Bruno Bombled⁵,
5 Jacqueline Boutin¹, Yann Bozec⁶, Steeve Comeau⁴, Pascal Conan^{7,8}, Laurent Coppola^{4,8}, Pascale Cuet⁹, Eva
6 Ferreira⁵, Jean-Pierre Gattuso^{4,10}, Frédéric Gazeau⁴, Catherine Goyet¹¹, Emilie Grosstefan¹², Bruno Lansard⁵,
7 Dominique Lefèvre¹³, Nathalie Lefèvre¹, Coraline Leseurre¹⁴, Sébastien Petton¹⁵, Mireille Pujo-Pay⁸, Christophe
8 Rabouille⁵, Gilles Reverdin¹, Céline Ridame¹, Peggy Rimmelin-Maury¹², Jean-François Ternon¹⁶, Franck
9 Touratier¹¹, Aline Tribollet¹, Thibaut Wagener¹³, Cathy Wimart-Rousseau¹⁷.

10
11 ¹ Laboratoire LOCEAN/IPSL, Sorbonne Université-CNRS-IRD-MNHN, Paris, 75005, France

12 ² OSU Ecce Terra, Sorbonne Université-CNRS, Paris, 75005, France

13 ³ Now at Institut des Sciences de la Terre, Grenoble, 38058, France

14 ⁴ Sorbonne Université, CNRS, Laboratoire d'Océanographie de Villefranche, LOV, F-06230 Villefranche-sur-
15 Mer, France

16 ⁵ Laboratoire des Sciences du Climat et de l'Environnement, LSCE/IPSL, UMR 8212 CEA- CNRS-UVSQ,
17 Université Paris-Saclay, 91191 Gif-sur-Yvette, France

18 ⁶ Station Biologique de Roscoff, UMR 7144 – EDYCO-CHIMAR, Roscoff, France

19 ⁷ Sorbonne Université, CNRS, Laboratoire d'Océanographie Microbienne, LOMIC, F-66650 Banyuls-sur-Mer,
20 France

21 ⁸ Sorbonne Université, CNRS OSU STAMAR - UAR2017, 4 Place Jussieu, 75252, Paris cedex 05, France

22 ⁹ Laboratoire ENTROPIE and Laboratoire d'Excellence CORAIL, Université de La Réunion-IRD- CNRS-
23 IFREMER-Université de la Nouvelle-Calédonie, 97744, Saint-Denis, La Réunion, France

24 ¹⁰ Institute for Sustainable Development and International Relations, Sciences Po, 27 rue Saint Guillaume, F-
25 75007 Paris, France

26 ¹¹ Espace-Dev UMR 228 Université de Perpignan Via Domitia, IRD, UM, UA, UG, 66860, Perpignan, France

27 ¹² Institut Universitaire Européen de la Mer (OSU-IUEM), Univ Brest, CNRS-UAR3113, 29280, Plouzané,
28 France

29 ¹³ Aix Marseille Univ, Université de Toulon, CNRS, IRD, MIO, Marseille, France

30 ¹⁴ Flanders Marine Institute (VLIZ), 8400 Ostend, Belgium

31 ¹⁵ Ifremer, Univ Brest, CNRS, IRD, LEMAR, F-29840 Argenton, France

32 ¹⁶ MARBEC, Univ Montpellier, CNRS, Ifremer, IRD, Sète, France

33 ¹⁷ National Oceanography Centre Southampton, European Way, Southampton, SO14 3ZH, UK

34
35 *Correspondence to:* Nicolas Metzl (nicolas.metzl@locean.ipsl.fr)
36

37 **Abstract.** Total alkalinity (A_T) and dissolved inorganic carbon (C_T) in the oceans are important properties to
38 understand the ocean carbon cycle and its link with global change (ocean carbon sinks and sources, ocean
39 acidification) and ultimately find carbon based solutions or mitigation procedures (marine carbon removal). We
40 present an extended database (SNAPO-CO2, Metzl et al, 2024d) with 24700 new additional data for the period
41 2002 to 2023. The full database now includes more than 67000 A_T and C_T observations along with basic
42 ancillary data (time and space location, depth, temperature and salinity) in various oceanic regions obtained since
43 1993 mainly in the frame of French research projects. This includes both surface and water columns data
44 acquired in open oceans, coastal zones, rivers and in the Mediterranean Sea and either from time-series or
45 punctual cruises. Most A_T and C_T data in this synthesis were measured from discrete samples using the same
46 closed-cell potentiometric titration calibrated with Certified Reference Material, with an overall accuracy of ± 4
47 $\mu\text{mol kg}^{-1}$ for both A_T and C_T . The same technique was used onboard for underway measurements during cruises
48 conducted in the Southern Indian and Southern Oceans. The A_T and C_T data from these cruises are also added in

49 this synthesis. The data are provided in one dataset for the global ocean (<https://doi.org/10.17882/102337>) that
50 offers a direct use for regional or global purposes, e.g. A_T /Salinity relationships, long-term C_T estimates,
51 constraint and validation of diagnostics C_T and A_T reconstructed fields or ocean carbon and coupled
52 climate/carbon models simulations, as well as data derived from Biogeochemical-Argo (BGC-Argo) floats.
53 These data can also be used to calculate pH, fugacity of CO_2 ($f\text{CO}_2$) and other carbon system properties to derive
54 ocean acidification rates or air-sea CO_2 fluxes.

55

56 **1 Introduction**

57

58 The ocean plays a major role in reducing the impact of climate change by absorbing more than 90% of
59 the excess heat in the climate system (Cheng et al., 2020, 2024; von Schuckmann et al, 2023; IPCC, 2022) and
60 about 25% of human released CO_2 (Friedlingstein et al., 2022, 2023). In the last decade, the oceans experienced
61 a rapid warming, the year 2023 being the hottest since 1955 (Cheng et al, 2024). In the atmosphere the CO_2
62 concentration continues its terrific progressive rising, reaching 419.3 ppm in 2023 (a rate of +2.83 ppm yr⁻¹, Lan
63 et al 2024). In August 2024, the global atmospheric CO_2 concentration was already above 420 ppm. In the next
64 decade the oceans will continue to capture heat and CO_2 , somehow limiting the climate change, but this oceanic
65 CO_2 uptake changes the chemistry of seawater reducing its buffering capacity (Revelle and Suess, 1957; Jiang et
66 al, 2023). This process known as ocean acidification has potential impacts on marine organisms (Fabry et al.,
67 2008; Doney et al., 2009, 2020; Gattuso et al., 2015). With atmospheric CO_2 concentrations, surface ocean
68 temperature and ocean heat content, sea-level, sea-ice and glaciers, the ocean acidification (decrease of pH) is
69 now recognized by the World Meteorological Organization as one of the 7 key properties for global climate
70 indicators (WMO, 2018). Ocean acidification is specifically referred in the SDG indicator 14.3.1 coordinated at
71 the Intergovernmental Oceanographic Commission (IOC) of UNESCO. Observing the carbonate system in the
72 open oceans, coastal zones and marginal seas and understanding how this system changes over time is thus
73 highly relevant not only to quantify the global ocean carbon budget, the anthropogenic CO_2 inventories or ocean
74 acidification rates, but also to understand and simulate the processes that govern the complex CO_2 cycle in the
75 ocean (e.g. Goyet et al, 2016, 2019) and to better predict the future evolution of climate and global changes
76 (Eyring et al., 2016; Kwiatkowski et al., 2020; Jiang et al., 2023). As the rate of change in ocean acidification
77 presents large temporal and regional variability, long-term observations are required. Weekly to monthly regular
78 resolution data are needed to better investigate the long-term change of the carbonate system in regions subject
79 to extreme events (e.g. tropical cyclones, marine heat or cold waves, rapid freshening, convection, dust events,
80 river discharges, etc....). In this context it is recommended to progress in data synthesis of the ocean carbon
81 observations that would offer new high quality products for the community (e.g. for GOA-ON, www.goa-on.org,
82 IOC/SDG 14.1.3, <https://oa.iode.org/>, Tilbrook et al., 2019).

83 In this work, following the first SNAPO-CO2 synthesis product (Metzl et al, 2024a), we present a new
84 synthesis of more than 67000 A_T and C_T data, measured either on shore or onboard Research Vessels obtained
85 over the 1993-2023 period during various cruises or at time-series stations mainly supported by French projects.
86 Hereafter this new dataset will be cited as SNAPO-CO2-v2. The methods, data assemblage and quality control
87 were presented in version V1. Here, we describe the new data added and discuss some potential uses of this
88 dataset.

89

90 2 Data collections

91

92 The time series projects and research cruises from which new data were collated are listed in Table 1
93 with information and references in the Supplementary file (Tables S1, S3 and S4). The sampling locations of
94 new data are displayed in Figure 1 (the location for all data presented in Figure S1). Sampling was performed
95 either from CTD-Rosette casts (Niskin bottles) or from the ship's seawater supply (intake at about 5m depth
96 depending on the ship and swell). Samples collected in 500 mL borosilicate glass bottles were poisoned with 100
97 to 300 μL of HgCl_2 depending on the cruises, closed with greased stoppers (Apiezon®) and held tight using
98 elastic band following the SOP protocol (DOE, 1994; Dickson et al., 2007). Some samples were also collected in
99 500 mL bottles closed with screw caps. After completion of each cruise, most of discrete samples were returned
100 back to the LOCEAN laboratory (Paris, France) and stored in a dark room at 4 °C before analysis generally
101 within 2-3 months after sampling (sometimes within a week). In this version we added data from samples that
102 were also returned to University of Perpignan or to University of La Réunion. In addition to discrete samples
103 analyzed for various projects conducted mainly in the North Atlantic, Tropical Atlantic, Mediterranean Sea and
104 coastal regions (Table 1), we complemented this second synthesis with A_T and C_T surface observations obtained
105 in the Indian and Southern oceans during the OISO cruises in 2019-2021 (Leseurre et al., 2022; Metzl et al,
106 2022; data also available at NCEI/OCADS: www.nodc.noaa.gov/ocads/oceans/VOS_Program/OISO.html) and
107 MINERVE cruises in 2002-2018 (Laika et al, 2009; Brandon et al, 2022). The A_T and C_T measurements from the
108 MINERVE cruises were performed either onboard R/V Astrolabe or back in the laboratories (at LOCEAN
109 laboratory and at University of Perpignan).

110

111

112

113

114

115

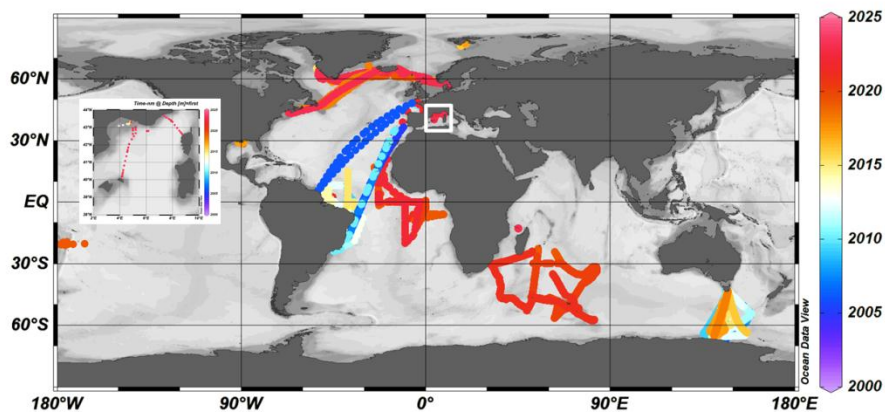
116

117

118

119

120



121

122

123

124

Figure 1: Locations of new A_T and C_T data (2005-2023) in the Global Ocean and the Western Mediterranean Sea (white box, insert) in the SNAPO-CO2-v2 dataset. Color code is for Year. Figure produced with ODV (Schlitzer, 2018).

125 **Table 1:** List of cruises added in the SNAPO-CO₂-v2 dataset. This is organized by region from North to South
 126 and the Mediterranean Sea. See Tables S1, S2, S3 and S4 in the Supplementary Material for a list of laboratories,
 127 of CRMs used, for DOI and for references of cruises. Nb = the number of data for each cruise or time-series. *
 128 indicates the measurements at sea (surface underway).

Cruise/Project	Start	End	Region	Sampling	Nb	
134	STEP	2016	2017	Arctic	Water Column	33
135	SURATLANT AX1	2017	2023	North Atlantic	Surface	255
136	SURATLANT AX2	2018	2023	North Atlantic	Surface	224
137	VOS	2005	2010	Atlantic	Surface	192
138	MISSRHODIA-1	2017	2017	Gulf Mexico	Water Column	8
139	ACIDHYPO	2022	2022	Gulf Mexico	Water Column	10
140	CAMFIN-WATL	2010	2015	Trop Atlantic	Surface	192
141	PIRATA-BR	2009	2015	Trop Atlantic	Surface	194
142	BIOAMAZON	2013	2014	Trop Atlantic	Surface	62
143	AMAZOMIX	2021	2021	Trop Atlantic	Water Column	180
144	PIRATA-FR	2019	2019	Trop Atlantic	Surface	93
145	PIRATA-FR	2020	2020	Trop Atlantic	Surface, Water Column	58
146	PIRATA-FR	2021	2021	Trop Atlantic	Surface, Water Column	79
147	PIRATA-FR	2022	2022	Trop Atlantic	Surface, Water Column	118
148	CO2ARVOR	2009	2010	Atlantic, Coastal	Surface, Water Column	621
149	SOMLIT-Roscoff	2020	2022	Coastal North Atl	Surface and 60m	207
150	SOMLIT-Brest	2020	2022	Coastal North Atl	Surface	251
151	TONGA	2019	2019	Trop Pacific	Water Column	226
152	CARBODISS	2018	2019	Indian Mayotte	Surface	85
153	OISO *	2019	2021	South Indian	Surface	5258
154	MINERVE	2004	2018	Southern Ocean	Surface	1077
155	MINERVE *	2002	2013	Southern Ocean	Surface	11258
156	COCORICO2	2017	2022	Coastal	Surface	589
157	SOMLIT-PointB	2019	2023	MedSea Coastal	Surface and 50m	716
158	SOLEMIO	2018	2022	MedSea Coastal	Water Column	271
159	ANTARES	2017	2023	MedSea	Water Column	506
160	MOLA	2018	2023	MedSea Coastal	Water Column	193
161	DYFAMED	2018	2023	MedSea	Water Column	514
162	MESURHO-BENT	2010	2011	MedSea Coastal	Surface and sub-surface	25
163	ACCESS-01	2012	2012	MedSea Coastal	Water Column	16
164	CARBO-DELTA-2	2013	2013	MedSea Coastal	Water Column	14
165	DICASE	2014	2014	MedSea Coastal	Water Column	22
166	MISSRHODIA-2	2018	2018	MedSea Coastal	Surface and sub-surface	13
167	DELTARHONE1	2022	2022	MedSea Coastal	Water Column	9
168	MOOSE-GE	2021	2021	MedSea	Water Column	451
169	MOOSE-GE	2022	2022	MedSea	Water Column	447
170	MOOSE-GE	2023	2023	MedSea	Water Column	475

171
172

173 3 Method, accuracy, repeatability and quality control

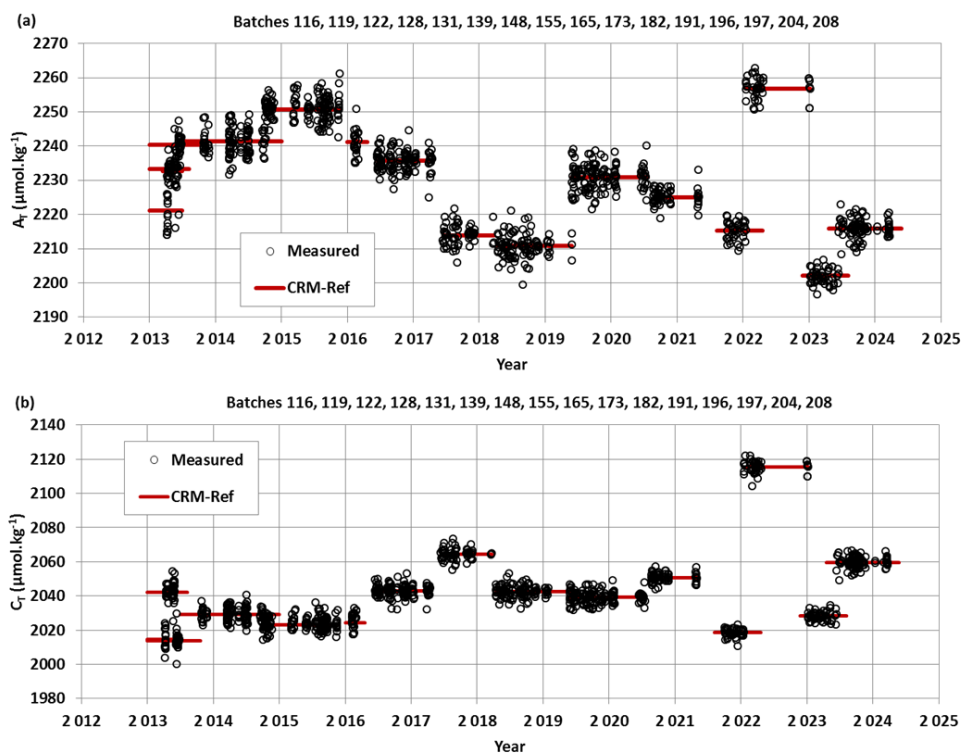
174

175 3.1 Method and accuracy

176

177 Since 2003, the discrete samples returned back at SNAPO-CO₂ Service facilities (LOCEAN, Paris),
 178 were analyzed simultaneously for A_T and C_T by potentiometric titration using a closed cell (Edmond, 1970;
 179 Goyet et al., 1991). The same technique was used at sea for surface water underway measurements during OISO
 180 and MINERVE cruises (indicated by * in Table 1). In the late 1980s the so-called “JGOFS-IOC Advisory Panel
 181 on Ocean CO₂” recommended the need for standard analysis protocols and for developing Certified Reference
 182 Materials (CRMs) for inorganic carbon measurements (Poisson et al., 1990; UNESCO, 1990, 1991). The CRMs

183 were provided to international laboratories by Pr. A. Dickson (Scripps Institution of Oceanography, San Diego,
 184 USA), starting in 1990 for C_T and 1996 for A_T , respectively. These CRMs were thus always available to us and
 185 used to calibrate the measurements (CRM Batch numbers used for each cruise are listed in the Supplementary
 186 file, Table S2). The CRMs accuracy, as indicated in the certificate for each Batch, is around $\pm 0.5 \mu\text{mol kg}^{-1}$ for
 187 both A_T and C_T (www.nodc.noaa.gov/ocads/oceans/Dickson_CRM/batches.html). The concentrations of CRMs
 188 we used vary between 2193 and 2426 $\mu\text{mol kg}^{-1}$ for A_T and between 1968 and 2115 $\mu\text{mol kg}^{-1}$ for C_T
 189 corresponding to the range of concentrations observed in open ocean water. In the Mediterranean Sea the
 190 concentrations are higher ($A_T > 2600 \mu\text{mol kg}^{-1}$ and $C_T > 2300 \mu\text{mol kg}^{-1}$) and in the coastal zones or near the
 191 Amazon River plume the concentrations were often lower than the CRMs ($A_T < 1500 \mu\text{mol kg}^{-1}$ and $C_T < 1000$
 192 $\mu\text{mol kg}^{-1}$). Results of analyses performed on 1242 CRM bottles (different Batches) in 2013-2024 are presented
 193 in Figure 2. The standard-deviations (Std) of the differences of measurements were on average $\pm 2.69 \mu\text{mol kg}^{-1}$
 194 for A_T and $\pm 2.88 \mu\text{mol kg}^{-1}$ for C_T . For unknown reasons, the differences were occasionally up to $10\text{-}15 \mu\text{mol kg}^{-1}$
 195 1 (1.2% of the data, Figure S2). These few CRM measurements were discarded for the data processing. We did
 196 not detect any specific signal for CRM analyses (e.g., larger uncertainty depending on the Batch number or
 197 temporal drifts during analyses, Figure 2) but for some cruises the accuracy based on CRMs could be better than
 198 $3 \mu\text{mol kg}^{-1}$ (e.g. $< 3 \mu\text{mol kg}^{-1}$ for AMAZOMIX cruise using 6 Batches #197 and for MOOSE-GE 2022 using
 199 19 Batches #204, or $< 1.5 \mu\text{mol kg}^{-1}$ for SOMLIT-Point-B in 2022 using 6 Batches #204).



220 **Figure 2:** A_T (a) and C_T (b) analyses for different CRM Batches measured in 2013-2024. For these 1242
 221 analyses the mean and standard-deviations of the differences with the CRM reference were $-0.11 (\pm 2.69) \mu\text{mol}$
 222 kg^{-1} for A_T and $0.01 (\pm 2.88) \mu\text{mol kg}^{-1}$ for C_T .

226 3.2 Repeatability

227

228 For some projects, duplicates have been regularly sampled (SOMLIT-Point-B, SOMLIT-Brest) or
229 replicate bottles sampled at selected depths at fixed stations during the cruises (e.g. STEP, CARBODISS). In the
230 first synthesis of the SNAPO-CO₂ dataset we showed the results from several time-series (SOMLIT-Point-B,
231 SOMLIT-Brest and BOUSSOLE/DYFAMED). Here we present the results for the new data obtained at
232 SOMLIT-Point-B in the coastal Mediterranean Sea and SOMLIT-Brest in the Bay of Brest (Figure 3). Results of
233 A_T and C_T repeatability are synthesized in Table 2. For the OISO cruises conducted in 2019, 2020 and 2021 the
234 repeatability was evaluated from duplicate analyses (within 20 minutes time) of continuous sea surface
235 underway sampling at the same location (when the ship was stopped). Similarly to what was found for the CRM
236 measurements (Figure S2), differences in duplicates are occasionally higher than 10-15 $\mu\text{mol kg}^{-1}$ (Figure 3) but
237 most of the duplicates for all projects are within 0 to 3 $\mu\text{mol kg}^{-1}$. Compared to previous results (Kapsenberg et
238 al. 2017; Metzl et al, 2024a), there are larger differences between duplicates at SOMLIT-B in 2019-2023 (up to
239 30 $\mu\text{mol kg}^{-1}$, Figure 3) leading to relatively large Std around 5 and 6 $\mu\text{mol kg}^{-1}$ for both A_T and C_T (Table 2).
240 The same was observed for duplicates at SOMLIT-Brest (Table 2). We do have not yet a clear explanation for
241 this large Std although larger variability was observed in recent years, and the measurements were performed
242 later after the sampling (e.g. more than 6 months for some samples during and after the COVID period). We will
243 see that given the temporal variability of the properties this does not lead to suspicious interpretation for the
244 seasonality or the trend analyses of these time-series.

245

246

247

248

249

250

251

252

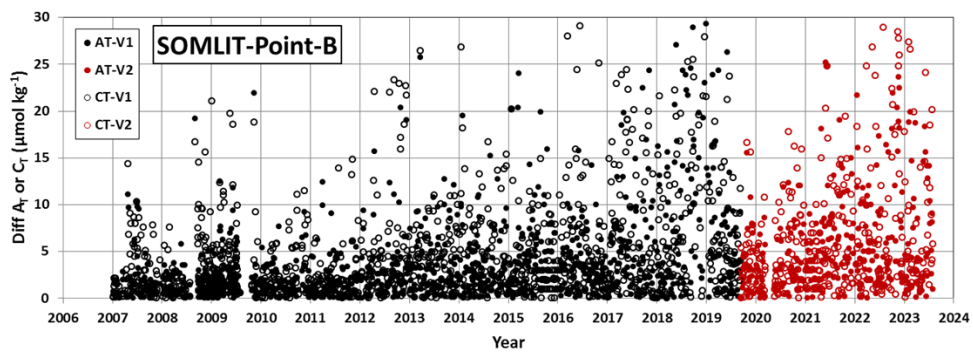


Figure 3: Results of duplicate A_T and C_T analyses from the time-series SOMLIT-Point-B in the coastal Mediterranean Sea and SOMLIT-Brest in the coastal Brittany for the data in the SNAPO-CO₂-v1 dataset (black) and new data added in SNAPO-CO₂-v2 (red). The plots show differences in duplicates for both A_T (filled circles) and C_T (open circles). Standard-deviations of these duplicates are listed in Table 2.

269 **Table 2:** Repeatability of A_T and C_T analyses for cruises with duplicate analysis. The results are expressed as the
 270 standard-deviations (Std) of the analysis of replicated samples. Nb = the number of replicates for each Time-
 271 series or Cruise. For the OISO cruises the mean repeatability was obtained from measurements at the same
 272 location (when the ship stopped).

Cruise	Period	Nb	Std A_T $\mu\text{mol kg}^{-1}$	Std C_T $\mu\text{mol kg}^{-1}$	Reference
STEP	2017	3	0.7	2.8	Unpublished
CARBODISS	2018	10	6.72	5.71	Unpublished
SOMLIT-Point-B	2007-2019	1130	4.5	5.1	SNAPO-CO2-v1, (a)
SOMLIT-Point-B	2019-2023	321	5.2	6.2	SNAPO-CO2-v2, (a)
SOMLIT-Brest	2008-2018	404	3.1	3.4	SNAPO-CO2-v1, (a)
SOMLIT-Brest	2019-2022	142	6.0	6.1	SNAPO-CO2-v2, (a)
OISO 29	2019	46	1.8	1.8	Leseurre et al (2022), (b)
OISO 30	2020	67	1.5	2.0	Metzl et al. (2022), (b)
OISO 31	2021	343	2.6	3.3	Metzl et al (2024c), (b)

292 (a) See Figure 3 for the results of regular duplicates for time-series SOMLIT-Point-B, SOMLIT-Brest.

293 (b) Metadata and data available at www.nodc.noaa.gov/ocads/oceans/VOS_Program/OISO.html

295 3.3 Assigned flags for quality control

296
 297 Identifying each data with an appropriate flag is very convenient for selecting the data (good,
 298 questionable or bad). Here we used 4 flags for each property (flags 2 = good, 3= questionable, 4=bad, and 9= no
 299 data) following the WOCE program and used in other data products such as SOCAT (Bakker et al., 2016) or
 300 GLODAP (Olsen et al., 2016; Lauvset et al., 2024). During the data-processing, we first assigned a flag for each
 301 A_T and C_T data based on the standard error in the calculation of A_T and C_T concentrations (non-linear regression,
 302 Dickson et al. 2007). By default, if the standard deviation on the regression is $> 1 \mu\text{mol kg}^{-1}$, we assigned a flag 3
 303 (questionable) although the data could be acceptable and then used for interpretations. Flag 3 was also assigned
 304 when salinity was doubtful or when differences of duplicates were large (e.g. $\pm 20 \mu\text{mol kg}^{-1}$). Flags 4 (bad or
 305 certainly bad) were assigned when clear anomalies were detected for unknown reasons (e.g. a sample probably
 306 not fixed with HgCl_2 or analysis performed late during the COVID issue). A secondary quality control was
 307 performed by the PIs of each project based on data inspection, duplicates, A_T /Salinity relationship, or the mean
 308 observations in deep layers where large variability in A_T and C_T is unlikely to occur from year to year.

309 An example for quality flag is presented for all data from the MINERVE cruises conducted in 2002-
 310 2018 in the Southern Ocean where clear outliers have been identified (Figure S3). For the MINERVE cruises in
 311 2002-2018 and a total of 12335 A_T and C_T analyses, 24 were identified as bad (flag 4), 978 for A_T and 971 for C_T
 312 listed as questionable (flag 3), and all others are considered as good data (flag 2, i.e. about 92%). For the
 313 MOOSE-GE cruises in 2021, 2022 and 2023 (new data in SNAPO-CO2-v2) and a total of 1373 A_T and C_T
 314 analyses, 2 were identified flagged as bad (flag 4), 38 for A_T and 33 for C_T listed as questionable (flag 3) all
 315 others were considered as good data (flag 2, i.e. 97%). This is better than the statistics we evaluated for the
 316 SNAPO-CO2-v1 dataset (90% flag 2 for MOOSE-GE in 2010-2019). A similar control was performed for each
 317 project.

318 **3.4 Inter-comparisons**

319

320 Inter-comparisons of measurements performed for different cruises or with different techniques help to
321 evaluate the quality of the data and detect potential biases when merging the data in the same region obtained by
322 different laboratories at different periods. This is especially important to interpret long-term trends of A_T and C_T
323 as well as for $p\text{CO}_2$ and pH calculated with A_T C_T pairs. The synthesis of various cruises in the same region and
324 periods also offers verification and secondary control of the data.

325

326 **3.4.1 Comparisons in deep layers**

327

328 Comparisons of data in the deep layers from different cruises are useful for secondary quality control as
329 one expects low natural variability or anthropogenic signals from season to season and over a few years. Several
330 cruises were conducted in the Mediterranean Sea in 2017-2023 (MOOSE-GE, ANTARES and DYFAMED). The
331 mean values of C_T and A_T in the deep layers ($> 1800\text{m}$) for each cruise confirmed the coherence of the data
332 (Table 3). The C_T and A_T concentrations are also in the range of the mean values evaluated for cruises conducted
333 in 2014 in the Mediterranean Sea (results listed in the SNAPO-CO₂-v1 synthesis, Metzl et al, 2024a). In the
334 western tropical Pacific we also observed coherent properties for the TONGA and OUTPACE cruises (Wagener
335 et al, 2018) for data selected at 1800-2300m layer corresponding to the C_T maximum layer in the Pacific Deep
336 Water (PDW). On the other hand in the western tropical Atlantic near the Amazon River plume where the spatial
337 variability of the properties is large at the surface (Ternon et al, 2000; Mu et al, 2021; Olivier et al, 2022) the
338 comparison in the water column is less clear (Figure S4). Nevertheless for the AMAZOMIX and the TARA-
339 Microbiome cruises, both conducted in September 2021, the results at close stations (around $5^\circ\text{N}/50^\circ\text{W}$) suggest
340 very similar concentrations at 1000m (Table 3). The comparisons in deep waters enabled to merge the different
341 datasets for interpretations of the temporal trends and processes driving the CO₂ cycle in these regions (e. g.
342 Ulses et al., 2023 and Wimart-Rousseau et al., 2023 for the Mediterranean Sea)

343

344 **3.4.2 Comparing on board and on shore results**

345

346 In surface waters where the variability is high inter-comparison is not relevant for secondary quality
347 control. However, during the MINERVE cruises, discrete samples were occasionally performed along with sea
348 surface underway measurements. Thus, we can compare A_T and C_T measured in the laboratory with those
349 measured onboard as described by Laika et al. (2009) for the MINERVE cruises in 2005-2006. It should be
350 noticed that the discrete samples were measured after a long trip (shipping boxes from Hobart, Tasmania to
351 Paris, France) and thus generally analyzed at least 3 months after the cruises (cruises conducted in October to
352 February, analyses performed in May-June). Given all the uncertainties associated to the sampling, samples
353 storage and transport, analyses and CRMs, the mean differences between discrete and underway data are still
354 reasonable (Std ranging between 4 and 12 $\mu\text{mol kg}^{-1}$, Table 4). For unknown reasons the mean difference was
355 high for a cruise in 2008-2009 (Std $> 10 \mu\text{mol kg}^{-1}$, the “weather goal”, Newton et al., 2015). With this in mind,
356 we believe the MINERVE data (both underway and discrete data) are useful to interpret the change of properties
357 in this region at seasonal or decadal scales (Laika et al., 2009; Brandon et al., 2022).

358

359 **Table 3:** Mean observations in the deep layers (> 1800m) of the Ligurian Sea (Western Mediterranean Sea for
360 different cruises conducted in 2017-2023), of the Tropical Pacific (around 2000m for cruises in 2017 and 2019),
361 and of the Tropical Atlantic (around 1000m for cruises in 2021). $N-A_T$ and $N-C_T$ are A_T and C_T normalized at
362 salinity ($S = 38$ in the Ligurian Sea; $S = 35$ for the Pacific and the Atlantic Oceans). Nb = number of data (with
363 flag 2). Standard deviations are in brackets.

Cruise	Period	Nb	Pot. Temp (°C)	Salinity	$N-A_T$ ($\mu\text{mol kg}^{-1}$)	$N-C_T$ ($\mu\text{mol kg}^{-1}$)
Ligurian Sea (> 1800m)						
All Cruises	2017-2023	227	12.923 (0.052)	38.484 (0.003)	2558.3 (10.5)	2300.0 (10.7)
DYFAMED	2017-2022	74	12.913 (0.006)	38.485 (0.002)	2555.1 (11.8)	2297.3 (12.4)
ANTARES	2017-2023	62	12.944 (0.096)	38.485 (0.005)	2559.8 (9.0)	2302.2 (8.9)
MOOSE-GE	2017-2023	91	12.917 (0.005)	38.484 (0.003)	2559.8 (9.8)	2300.7 (10.0)
Tropical Pacific (layer 1800-2300m)						
OUTPACE	2017	15	2.124 (0.055)	34.633 (0.006)	2414.1 (8.0)	2318.8 (5.8)
TONGA	2019	7	2.196 (0.197)	34.619 (0.016)	2408.9 (9.1)	2327.2 (7.5)
Western Tropical Atlantic (1000m)						
AMAZOMIX	2021	14	4.770 (0.105)	34.711 (0.041)	2315.6 (20.2)	2220.8 (17.1)
TARA-MICRO	2021	1	4.852	34.717	2312.9	2231.1

402 **Table 4:** Comparison of A_T and C_T analysed on-board and at SNAPO-CO2 facilities for the MINERVE project.
403 The results are expressed as the standard deviations (Std) of the differences for each cruise. Nb = the number of
404 co-located samples.

Period	Nb	Std A_T $\mu\text{mol kg}^{-1}$	Std C_T $\mu\text{mol kg}^{-1}$
2004-2005	109	12.85	4.99
2005-2006	45	4.20	6.77
2007-2008	17	10.15	10.62
2008-2009	26	15.80	12.02
2009-2010	22	4.04	5.78
2010-2011	33	9.36	6.83
2012-2013	29	5.43	9.73

3.4.3 Comparison based on different techniques

Another example of comparison is presented for samples obtained in the lagoon of Mayotte Island in the western Indian Ocean and measured using different techniques. In the frame of the CARBODISS project seawater was sampled in 2018-2023 at several coral reef sites within the north-eastern part of the lagoon and measured either at LOCEAN laboratory or at La Réunion University. To remove coral sand particles the water samples were immediately filtered through Whatman GF/F filters and poisoned with mercuric chloride, following Dickson et al. (2007). In 2021, 2022 and 2023, A_T was measured at La Réunion University using an automated potentiometric titration (905 Titrandro Metrohm titrator with combined pH electrode 6.0253.00) and calculated from the second inflection point of the titration curve. The HCl concentration was checked each day of measurements using a CRM provided by A. Dickson, Scripps Institution of Oceanography. The A_T precision of $\pm 2 \mu\text{mol kg}^{-1}$ was based on triplicate analyses (Lagoutte et al., 2023). In the studied coral reef sites A_T concentrations ranged between 2250 and 2350 $\mu\text{mol kg}^{-1}$ but with occasional higher concentrations up to 2450-2500 $\mu\text{mol kg}^{-1}$. Such high A_T has been observed in other coral reefs ecosystems (Cyronak et al., 2013 at Cook Island; Palacio-Castro et al., 2023 at Middle Keys, Florida). The data obtained in the lagoon of Mayotte on different coral reefs could be compared with underway observations obtained offshore of Mayotte Island (OISO-11 cruises in 2004 and CLIM-EPARSEs cruise in 2019, data available in the SNAPO-CO2-v1 dataset). In the open ocean the A_T concentrations ranged between 2250 and 2330 $\mu\text{mol kg}^{-1}$, close to the results obtained at Mayotte reefs except for samples in November 2021 that were all collected at Cratère station (12.84°S-45.39°E) (Figure 4). At this location there was a large diurnal variation in November 2021 with A_T increasing from 2322 to 2508 $\mu\text{mol kg}^{-1}$ (Figure S5). This is because in 2021 the samples were taken at low tide recording a volcanic signal at this site allowing recording for the first time the volcanic signal in this location (CO_2 resurgences). In 2018 and 2019 such high A_T were not measured (Figure S5) as samples were taken at high tides allowing a certain dilution of volcanic CO_2 emissions in the water column. Although the samples were measured with different techniques the range of A_T is coherent for both datasets (Figure 4). Therefore we added the A_T data measured at La Réunion University in 2021-2023 to complete the synthesis for this location (Mayotte Island).

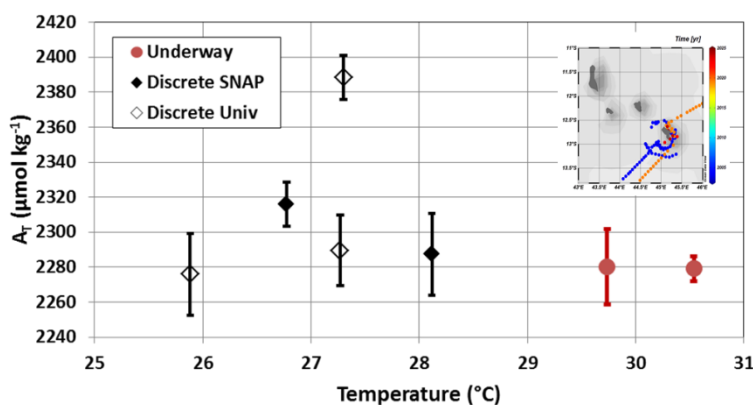


Figure 4: Total alkalinity (A_T) versus temperature for samples measured around Mayotte and in the coral reef (insert map). Underway A_T was measured onboard in 2004 and 2019 (red circles) whereas discrete samples at different reef sites within the lagoon of Mayotte in 2018, 2019, 2021, 2022 and 2023 were measured at LOCEAN (black diamonds) or at La Réunion University (open diamonds). The figure presents the data averaged for each cruise in this region.

466 **3.4.4 Summary of quality control data**

467

468 The total number of data in the SNAPO-CO2-v2 dataset for the Global Ocean is gathered in Table 5
 469 with corresponding flags for each property. Overall, the synthesis includes more than 91% of good data for both
 470 A_T and C_T . About 6% are questionable and 3% are likely bad. Overall, we believe that all data (with flag 2) in
 471 this synthesis have an accuracy better than $4 \mu\text{mol kg}^{-1}$ for both A_T and C_T , the same as for quality-controlled
 472 data in GLODAP (Lauvset et al., 2024). The uncertainty ranges between the “Climate goal” ($2 \mu\text{mol kg}^{-1}$) and
 473 the “Weather Goal” ($10 \mu\text{mol kg}^{-1}$) for ocean acidification studies (Newton et al., 2015; Tilbrook et al., 2019).
 474 This accuracy is also relevant to validate or constraint data-based methods that reconstruct A_T and C_T fields with
 475 an error of around 10-15 $\mu\text{mol kg}^{-1}$ for both properties (Bittig et al., 2018; Broullón et al., 2019, 2020; Fourier et
 476 al., 2020; Gregor and Gruber, 2021; Chau et al., 2024a).

477

478

479 **Table 5:** Number of Temperature, Salinity, A_T and C_T data in the SNAPO-CO2-v2 synthesis identified for flags
 480 2 (good), 3 (questionable), 4 (bad), 9 (no data). Last column is the percentage of flag 2 (Good).

481

482

Property	Flag 2	Flag 3	Flag 4	Flag 9	% flag 2
Temperature	68253	418	0	653	99.4
Salinity	68706	482	5	131	99.3
A_T	61249	3910	2077	2088	91.1
C_T	61869	3865	2057	1533	91.3

490

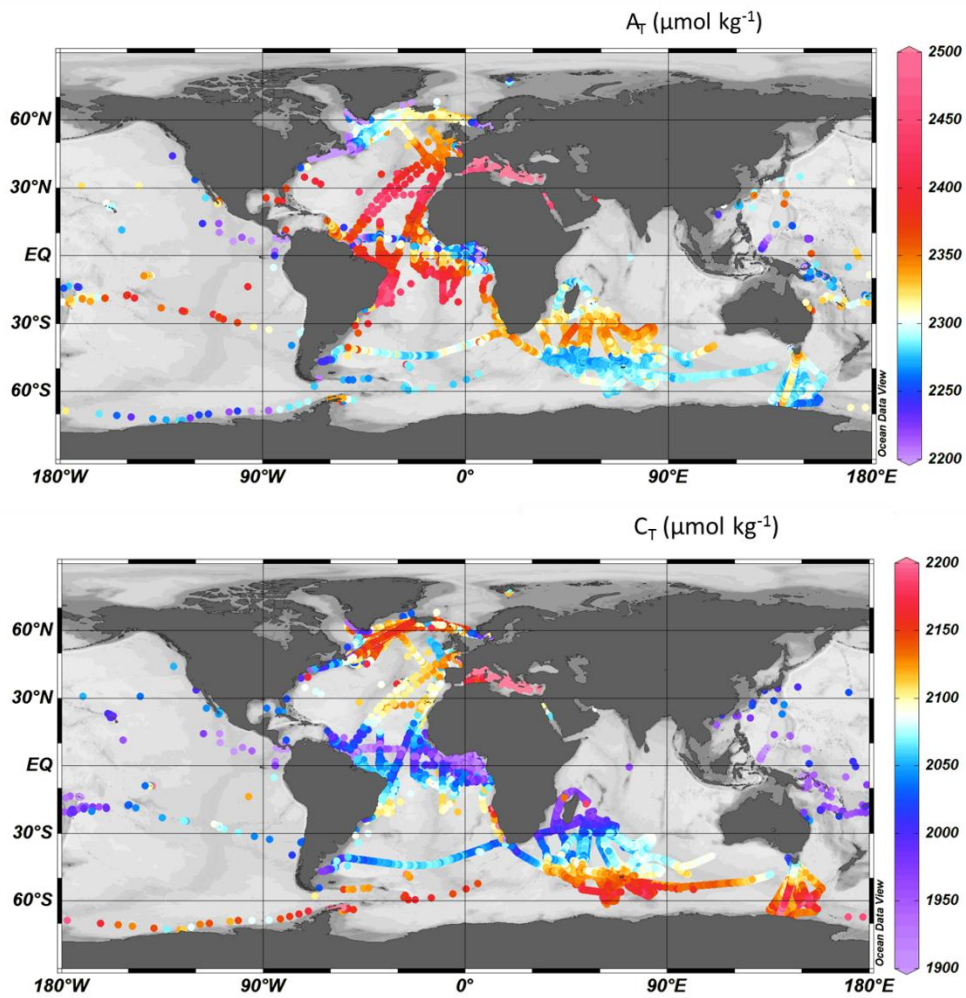
491

492 **4 Global A_T and C_T distribution based on the SNAPO-CO2-v2 dataset**

493

494 The surface distribution in the global ocean based on the SNAPO-CO2 dataset is presented in Figure 5
 495 for A_T and C_T . The A_T /Salinity and A_T / C_T relationships are clearly identified and structured at regional scale
 496 (Figure 6). In the open ocean, high A_T concentrations ($> 2400 \mu\text{mol kg}^{-1}$) are identified in the Atlantic subtropics
 497 (bands 35°N - 15°N and 25°S - 3°S) (Jiang et al., 2014; Takahashi et al., 2014). The lowest A_T and C_T
 498 concentrations ($< 600 \mu\text{mol kg}^{-1}$) are observed in the western tropical Atlantic in the Amazon River plume near
 499 the mouth (Lefèvre et al., 2017b). For C_T the concentrations are high ($> 2150 \mu\text{mol kg}^{-1}$) in the Southern Ocean
 500 south of the polar front, associated with the deep mixing in winter and the upwelling of deep water (Metzl et al.,
 501 2006; Pardo et al., 2017). The highest C_T concentrations (up to 2180-2270 $\mu\text{mol kg}^{-1}$) are observed in the high
 502 latitudes of the Southern Ocean near the Adélie coastal zone (MINERVE and ACE cruises), around the
 503 Kerguelen plateau (OISO-31 cruise) and close to the Antarctic Peninsula (TARA-Microbiome cruise). In the
 504 North Atlantic the new data from SURATLANT cruises in 2018-2023 confirm the high C_T concentrations ($>$
 505 $2150 \mu\text{mol kg}^{-1}$) observed in the Sub-polar gyre since 2016 due in part to the accumulation of anthropogenic CO_2
 506 (Leseurre et al., 2020). Low C_T concentration ($< 2000 \mu\text{mol kg}^{-1}$) are found in the tropics (10°N - 30°S) with
 507 lower values ($< 1950 \mu\text{mol kg}^{-1}$) in the equatorial Atlantic band 10°N -Eq (e.g. Koffi et al., 2010; Lefèvre et al.,
 508 2021). In the Amazon shelf sector C_T can reach even lower concentration ($< 1700 \mu\text{mol kg}^{-1}$, AMAZOMIX
 509 cruise).

510
511
512
513
514
515
516
517
518
519
520
521
522
523
524
525
526
527
528
529
530
531
532
533
534
535
536
537
538



539
540
541
542
543
544
545
546
547
548
549
550
551
552
553
554
555
556
557
558
559
560
561
562
563

Figure 5: Distribution of A_T (top) and C_T (bottom) concentrations ($\mu\text{mol.kg}^{-1}$) in surface waters (0-10m) in the SNAPO-CO2-v2 dataset. Only data with flag 2 are presented in these figures. Figures produced with ODV (Schlitzer, 2018).

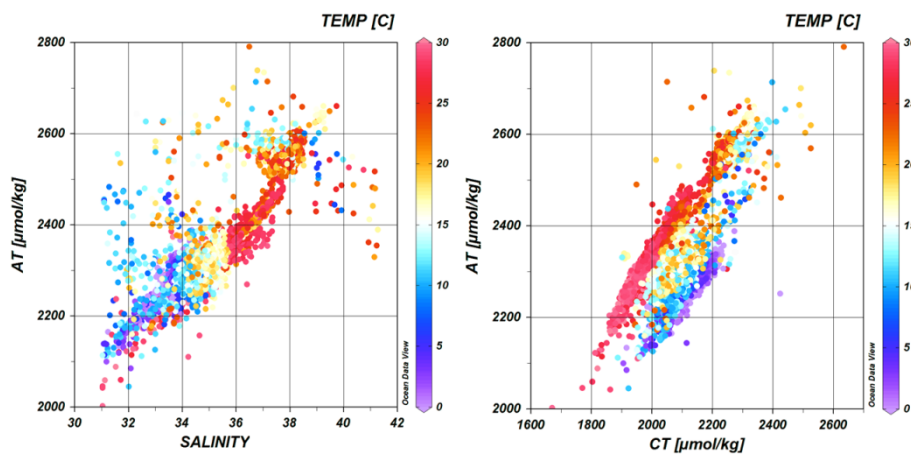


Figure 6: Relationships between A_T and Salinity (left panel) and A_T versus C_T (right panel) for samples in surface waters (0-10m and Salinity > 31). Only data with flag 2 are presented (nb = 48749). The color scales correspond to the temperature. The data not aligned correspond to coastal zones (e.g. COCORICO2 stations). Figures produced with ODV (Schlitzer, 2018).

564
565
566
567
568
569
570
571
572
573
574
575
576
577
578
579
580
581
582
583
584
585
586
587
588
589
590
591
592
593
594
595
596
597
598
599
600
601
602
603
604

5 Regional A_T and C_T distributions and trends based on the SNAPO-CO2 dataset

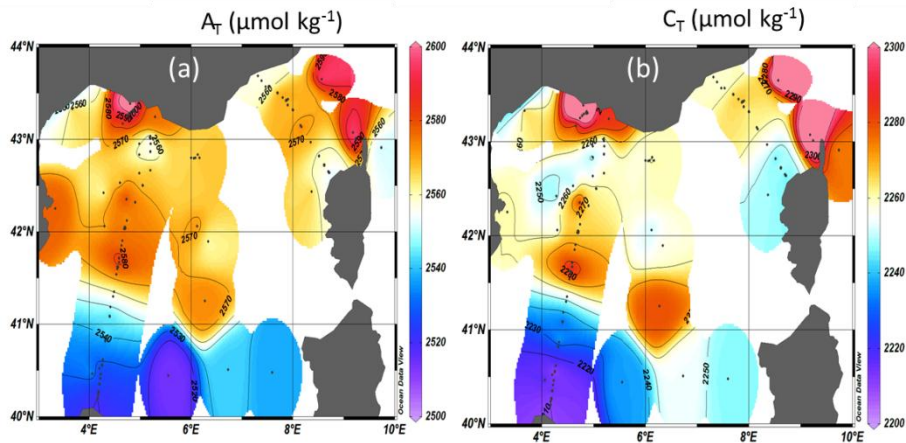
The regional distributions are described for the Mediterranean Sea and for selected regions in the open ocean and coastal zones where the data are available for 10 years or more to explore the A_T and C_T trends. Given the observed seasonal and inter-annual variability and that the time-series were not regular (e.g. at monthly frequency), we cannot use recommended methods to estimate the trends (e.g. based on de-seasoned data, Sutton et al, 2022). Here we have selected the locations and seasons where the C_T trends can be linearly fitted and compared with no interpolation to fill gaps and discontinuous data (e.g., fewer samples during the COVID period).

5.1 The Mediterranean Sea

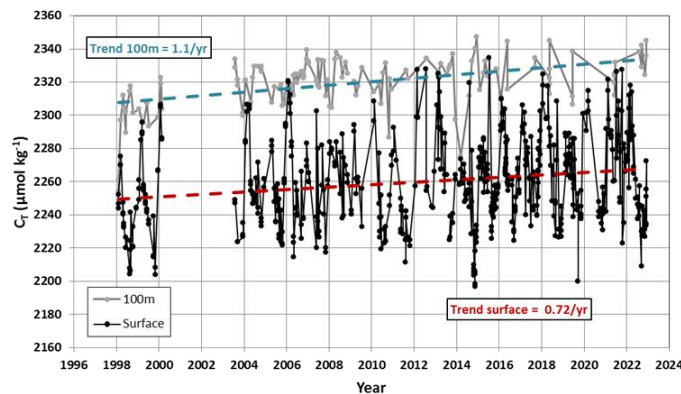
Compared to the open ocean, A_T concentrations are much higher in the Mediterranean Sea (Copin-Montégut, 1993; Schneider et al., 2007; Álvarez et al., 2023) with values up to $2600 \mu\text{mol kg}^{-1}$. The A_T and C_T data obtained in 2014-2023 show a clear contrast between the northern and southern regions of the Western Mediterranean Sea with higher concentration in the Ligurian Sea and the Gulf of Lion (Figure 7). This contrast is associated to the circulation and the frontal system in this region (e.g. Barral et al, 2021). New data in the coastal zones in the Gulf of Lion (ACCESS, DICASE, CARBODELTA, COCORICO2, MESURHOBENT) also have very high A_T and C_T concentrations ($A_T > 2600 \mu\text{mol kg}^{-1}$; $C_T > 2350 \mu\text{mol kg}^{-1}$). Very low A_T and C_T concentrations ($A_T < 2500 \mu\text{mol kg}^{-1}$; $C_T < 2200 \mu\text{mol kg}^{-1}$) were also occasionally observed in the coastal zones (COCORICO2 stations, Petton et al, 2024).

In summer 2022 the Mediterranean Sea experienced an exceptional warming (Figure S6) superposed to the long-term warming in the ocean (Cheng et al, 2024). Such event would impact the internal ocean processes such as thermodynamic, stratification and biological processes (Coppola et al., 2023) and the inter-annual variability and trends of C_T , pH, $f\text{CO}_2$ and air-sea CO_2 fluxes (Yao et al., 2016; Wimart-Rousseau et al., 2023; Chau et al., 2024b). As in 2003, the warming in summer 2022 was associated to the drought event that occurred in Europe and over the Mediterranean Sea (Faranda et al., 2023). In July 2022, the maximum temperature of 28.42°C was observed at station SOMLIT-Point-B. In the Ligurian Sea the temperature trend was faster in recent years, $+0.173 \pm 0.072 \text{ }^\circ\text{C}$ per decade over 1990-2010 and $+0.678 \pm 0.143$ per decade over 2010-2023 (Figure S6). With the new data added in the SNAPO-CO2-v2 synthesis (DYFAMED, MOOSE-ANTARES, and MOOSE-GE) we evaluated a temperature trend of $+0.84 \pm 0.20 \text{ }^\circ\text{C}$ per decade over 1998-2022 indicating that the discrete sampling captured the property changes at regional scale. Based on the data in the Ligurian Sea the trends of C_T appeared faster in summer ($+1.53 \pm 0.46 \mu\text{mol kg}^{-1} \text{ yr}^{-1}$) than in winter ($+0.94 \pm 0.64 \mu\text{mol kg}^{-1} \text{ yr}^{-1}$, Table 6). On the other hand, the trends of A_T were the same ($+0.72 \pm 0.36 \mu\text{mol kg}^{-1} \text{ yr}^{-1}$ in winter and $+0.69 \pm 0.42 \mu\text{mol kg}^{-1} \text{ yr}^{-1}$ in summer). The trend of C_T in surface in winter was close to the one derived at 100m (below the Chl-a maximum), $C_T^{100\text{m}} = +1.10 \pm 0.17 \mu\text{mol kg}^{-1} \text{ yr}^{-1}$ (Figure 8) whereas for A_T the trend was the same in surface and at depth ($+0.76 \pm 0.12 \mu\text{mol kg}^{-1} \text{ yr}^{-1}$). This suggests that the winter C_T data recorded the anthropogenic CO_2 uptake of around $+1 \mu\text{mol kg}^{-1} \text{ yr}^{-1}$, Figure S7). Note that, given the observed C_T trends, the spatial view presented in Figure 7b for 2014-2023 would be the same based on C_T concentrations normalized to a reference year. As noted by Touratier and Goyet (2009) the C_T concentrations in the Mediterranean Sea should

605 increase in parallel with the level of atmospheric anthropogenic CO₂. For an atmospheric CO₂ rate of +2.16 ppm
 606 yr⁻¹ over 1998-2023 (Lan et al., 2024) and at fixed sea surface temperature (17.75°C), salinity (38.25) and A_T
 607 (2567 μmol kg⁻¹), the theoretical C_T increase would be +1.24 μmol kg⁻¹ yr⁻¹. Interestingly, an anthropogenic flux
 608 of -0.3 ± 0.02 molC m⁻² yr⁻¹ in the Mediterranean Sea (Bourgeois et al., 2016) would correspond to an increase of
 609 C_T of 1.07 ± 0.07 μmol kg⁻¹ yr⁻¹ in the top 100 meters. This is again close to what is observed in winter or at
 610 100m (Table 6, Figure 8). On the other hand the faster C_T trend observed in surface waters during summer might
 611 be associated with a decrease in biological production and/or changes in circulation/mixing over time that
 612 deserve specific investigations such as analyzed for the oxygen budget in this region (Ulses et al, 2021). It is
 613 worth noting that the C_T and A_T trends in coastal zones of the Mediterranean Sea are opposite to those observed
 614 offshore: for example at station SOLEMIO (Bay of Marseille, Wimart-Rousseau et al., 2020) the C_T and A_T
 615 concentrations decreased over 2016-2022 and thus opposed to the anthropogenic CO₂ signal, indicating that
 616 processes such as riverine inputs, advection or biology control the carbonate system decadal variability at local
 617 scale. This calls for developing dedicated complex biogeochemical models to resolve these processes (Barré et
 618 al., 2023, 2024), especially when extreme events occurred, such as the very hot summer in 2024 with SST up to
 619 30°C in the Mediterranean Sea (Platforms Buoy/Mooring AZUR, EOL and La Revellata, data available at
 620 <https://dataselection.coriolis.eu.org/>). The data obtained in the Mediterranean Sea are important not only to
 621 validate biogeochemical models but also to reconstruct the carbonate system from A_T and pCO₂ data (Chau et al.,
 622 2024a) as the global A_T/SSS relationships (e.g. Carter et al., 2018) are not suitable for this region.



634 **Figure 7:** Distribution of A_T (a) and C_T (b) in μmol kg⁻¹ in surface waters of the Mediterranean Sea (0-10m) from
 635 observations over 2014-2023. Figures produced with ODV (Schlitzer, 2018).



651
652 Figure 8: Time-series of C_T concentrations in surface (black symbols) and at 100m (grey symbols) in the
653 Ligurian Sea. The trends over 1998-2022 is surface (red) and at 100m (blue) are indicated by dashed lines.
654

655 5.2 The North Atlantic

656
657 The North Atlantic Ocean is an important CO_2 sink (Takahashi et al. 2009) due to biological activity
658 during summer, heat loss and deep convection during winter. As a result this region contains high concentrations
659 of anthropogenic CO_2 (C_{ant}) in the water column (Khatiwala et al., 2013). Decadal variations of the C_{ant}
660 inventories were recently identified at basin scale probably linked to the change of the overturning circulation
661 (Gruber et al., 2019; Müller et al., 2023; Pérez et al., 2024). This region experienced climate modes such as the
662 North Atlantic Oscillation (NAO) and the Atlantic Multidecadal Variability (AMV) that imprint variability in
663 air-sea CO_2 fluxes at inter-annual to multidecadal scales (e.g. Thomas et al., 2008; Jing et al., 2019;
664 Landschützer et al., 2019) but not always clearly revealed at regional scale (Metzl et al., 2010; Schuster et al.,
665 2013; Pérez et al., 2024). In addition it has been recently shown that extreme events such as the marine heat
666 wave in summer 2023 led to a reduce CO_2 uptake in this region (Chau et al., 2024b). Although the annual
667 CO_2 fluxes deduced from Global Ocean Biogeochemical Models (GOBM) seem coherent with the data-products
668 at basin scale (resp. -0.30 ± 0.07 and -0.24 ± 0.03 PgC/yr for the North Atlantic subpolar seasonally stratified,
669 NA-SPSS biome) the pCO_2 cycle seasonality is not well simulated (Pérez et al., 2024). Therefore to correct the
670 GOBMs outputs, comparisons with the observed C_T and A_T cycles are also needed.

671 In this context regular sampling in the North Atlantic (OVIDE cruises, Mercier et al., 2015, 2024;
672 SURATLANT transects, Reverdin et al., 2018) and time-series stations in the Irminger and Iceland Seas
673 (Ólafsson, et al., 2010; Lange et al., 2024; Yoder et al., 2024) are important to explore the variability of the
674 biogeochemical properties from seasonal (Figure S8) to decadal scales (Figure 9). The SURATLANT data added
675 in the SNAPO-CO2-v2 dataset over 2017-2023 offer new observations in the North Atlantic Subpolar Gyre
676 (NASPG in the NA-SPSS biome) and new transects from Norway to Iceland and reaching the coast of Greenland
677 (Figure 9). In 2010 the winter NAO was negative, moved to a positive state in 2012-2020 and was again very
678 low in 2021. The new SURATLANT data after 2017 confirm the cooling and the freshening in the NASPG since
679 2009 (Holliday et al., 2020; Leseurre et al., 2020; Siddiqui et al., 2024) whereas the most recent data in 2022 and
680 2023 suggest a reverse trend (increase of salinity and temperature, Figure S8). After 2016, large C_T anomalies in
681 the NASPG were observed. For examples, in April 2019 and 2022, the C_T concentrations were low compared to
682 2016 (Figure 9) and opposed to the expected anthropogenic CO_2 uptake. In September 2023 the C_T
683 concentrations were much lower than in 2022 (Figure 9) probably linked to biological productivity when the
684 NAO index was negative (Fröb et al., 2019) as observed in summer 2023 (NAO < -2 in July 2023). Despite these
685 variability the C_T trends are relatively well evaluated (Table 6). As in the Mediterranean Sea the C_T trends in the
686 NASPG appeared different depending on the season (Figure 9). The C_T increase was faster in September than in
687 April (resp. $+1.09 \pm 0.37 \mu mol kg^{-1} yr^{-1}$ and $+0.78 \pm 0.23 \mu mol kg^{-1} yr^{-1}$). This is either close to or lower than the
688 theoretical C_T increase due to the rising of atmospheric CO_2 ($+0.91 \mu mol kg^{-1} yr^{-1}$) and in the range of recent
689 results evaluated for the Sub-polar Mode Waters in the Irminger Sea (C_{ant} trend = $0.95 \pm 0.17 \mu mol kg^{-1} yr^{-1}$ for
690 the period 2009-2019, Curbelo-Hernández et al., 2024).

691

692
693
694
695
696
697
698
699
700
701
702
703
704
705
706

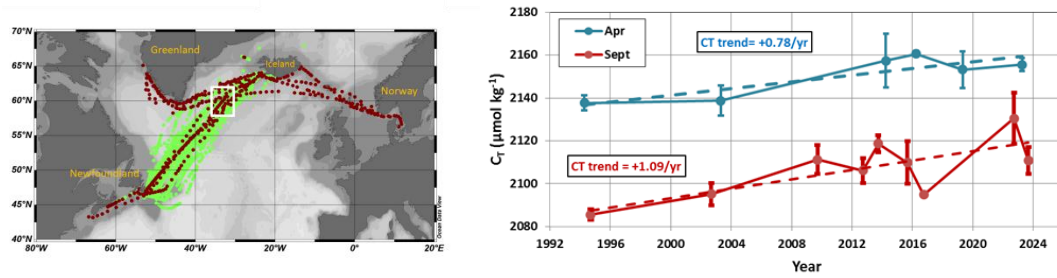


Figure 9: Left: Data in SNAPO-CO2-v1 (green) and new data in v2 (brown) from the SURATLANT cruises in 1993-2023 in the North Atlantic. Figure produced with ODV (Schlitzer, 2018). The white box identified the region of selected data around 60°N for the trend analysis. Right: Time-series of average C_T concentrations in April (blue) and September (red) in this region. The trends for each season are indicated (see also Table 6).

707 5.3 The Tropical Atlantic

708

709 In the Tropical Atlantic, previous studies highlighted the large variability of biogeochemistry and the
710 difficulty in detecting long-term trends of C_T (e.g. Lefèvre et al., 2021). This is related to the variability of
711 circulation, equatorial upwelling, biological processes (some linked to Saharan dust) and inputs from large rivers
712 (Congo, Amazon and Orinoco). The new data added in version SNAPO-CO2-v2 (Figure S9) show the
713 contrasting zonal C_T distribution in this region with lower concentrations in low salinity regions of the North
714 Equatorial Counter Current and Guinea Current (Figure 5; Oudot et al., 1995; Takahashi et al., 2014; Broullón et
715 al., 2020; Bonou et al., 2022). For exploring the temporal changes we selected the data in the western region
716 available for at least 10 years and separated the northern and southern sectors. In both regions the C_T trend is
717 close to $+3 \mu\text{mol kg}^{-1} \text{ yr}^{-1}$ (Table 6, Figure S9) much higher than the expected anthropogenic signal. In this
718 region where coastal water masses mixes with oceanic waters, the inter-annual variability of C_T is large and the
719 changes driven by competitive processes (circulation, biological processes). More observations and dedicated
720 models are needed to separate the anthropogenic and natural variability in this region (Pérez et al., 2024).

721

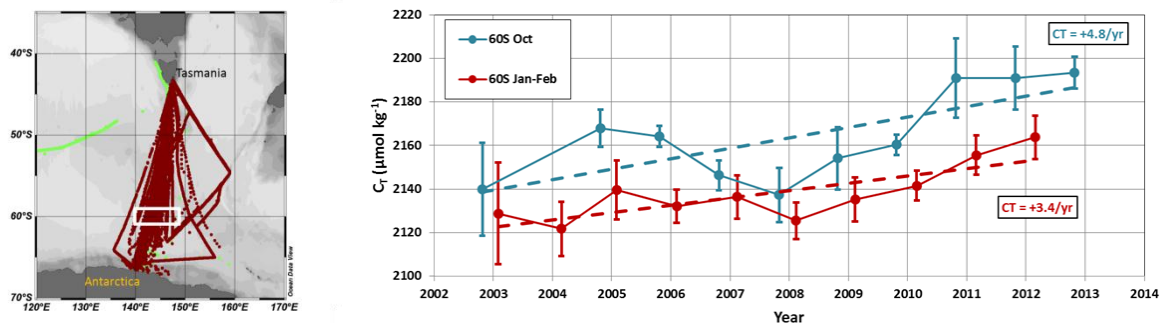
722 5.4 The Southern Ocean

723

724 In the Southern Ocean there are a few regular multi-annual observations of the carbonate system. Time
725 series of more than 10 years were obtained in the Drake Passage (Munro et al., 2015) and in the Southern Indian
726 Ocean (Leseurre et al., 2022; Metzl et al., 2024b). Observations were also obtained for more than 20 years
727 southeast of New Zealand at the Munida Time Series (MTS) in the subtropical and sub-Antarctic frontal zones
728 (Currie et al., 2011; Vance et al., 2024). To complement these datasets we have added the data collected in the
729 South-Eastern Indian Ocean between Tasmania and Antarctica in the frame of the MINERVE cruises (Figure 10;
730 Brandon et al., 2022). These cruises were conducted from October to March offering each year a view of the
731 seasonal changes between late winter and summer from the sub-Antarctic zone to the coastal zone near
732 Antarctica (Adélie land). In all sectors (here from 45°S to 67°S) the C_T concentrations were higher in October
733 when the mixed-layer depth (MLD) was deep and were lower during the productive summer season (e.g. Laika
734 et al., 2009; Shadwick et al., 2015). An example is presented at 60°S/151°E from the data obtained along a
735 reoccupied track in 2011-2012 (Figure S10). At this location south of the Polar Front in the POOZ/HNLC area

736 (Permanent Open Ocean Zone/ High Nutrient Low Chlorophyll), the C_T concentrations were $+25 \mu\text{mol kg}^{-1}$
 737 higher in October compared to February. The same seasonal amplitude was observed in the western Indian sector
 738 of the POOZ (Metzl et al., 2006, 2024b) suggesting that the C_T seasonality is relatively homogeneous in this
 739 region corresponding to the Indian SO-SPSS biome (Fay and McKinley, 2014). The difference in the
 740 climatological C_T between October and January is on average $+28.3 \pm 9.8 \mu\text{mol kg}^{-1}$ in the Indian Ocean POOZ
 741 (Takahashi et al., 2014). Given this seasonality and potential change in the seasonal amplitude over time
 742 (Gallego et al., 2018; Landschützer et al., 2018; Shadwick et al., 2023) the property trends have to be evaluated
 743 for October and January-February separately, here over 2002-2012 in the POOZ (Figure 10, Table 6). In both
 744 seasons, the average C_T concentrations reached a minimum in 2008 and increased faster in 2008-2012 (up to
 745 $+4.8 \mu\text{mol kg}^{-1} \text{yr}^{-1}$). Interestingly, such acceleration of the trend after 2009 was observed for $p\text{CO}_2$ at the MTS
 746 station (Vance et al., 2024). We note that the C_T trend over 2002-2012 was slightly faster in October (Figure 10)
 747 probably linked to deeper MLD as suggested from the cooling and the salinity increase observed during this
 748 season (Figure S10).

749
750
751
752
753
754
755
756
757
758
759
760



761 **Figure 10:** Left: Data in SNAPO-CO2-v1 dataset (green) and new data in version v2 (brown) in the South
 762 eastern Indian Ocean. Figure produced with ODV (Schlitzer, 2018). The white box identified the region of
 763 selected data around 60°S for the trend analysis. Right: Time-series of average C_T concentrations in January-
 764 February (red) and October (blue) around 60°S (white box in the map). The trends for each season are indicated
 765 (see also Table 6).

766
767
768
769
770
771
772
773
774

In the western Indian sector, the new data in the SNAPO-CO2-v2 dataset from the OISO cruises at high
 latitudes also recorded a rapid C_T trend over 5-8 years periods (e.g., $+3.4 \mu\text{mol kg}^{-1} \text{yr}^{-1}$ in 2015-2020 at 56°S,
 Figure 11, Table 6). Although the inter-annual variability of C_T , between 10 and 20 $\mu\text{mol kg}^{-1}$, is often
 recognized (Figure 11), the evaluation of the trends over more than 20 years indicated faster trend in the
 subtropical Indian Ocean ($+1.1 \mu\text{mol kg}^{-1} \text{yr}^{-1}$) compared to higher latitudes (Indian POOZ, $+0.6 \mu\text{mol kg}^{-1} \text{yr}^{-1}$);
 they are close to the expected anthropogenic signal in these regions ($+1.1 \mu\text{mol kg}^{-1} \text{yr}^{-1}$ in the subtropics and
 $+0.8 \mu\text{mol kg}^{-1} \text{yr}^{-1}$ at higher latitudes).

775
776
777
778
779
780
781
782
783
784
785
786
787
788
789
790
791
792
793
794
795
796
797
798
799
800
801
802
803
804
805
806
807
808
809
810
811
812
813
814
815
816
817
818
819
820
821
822
823

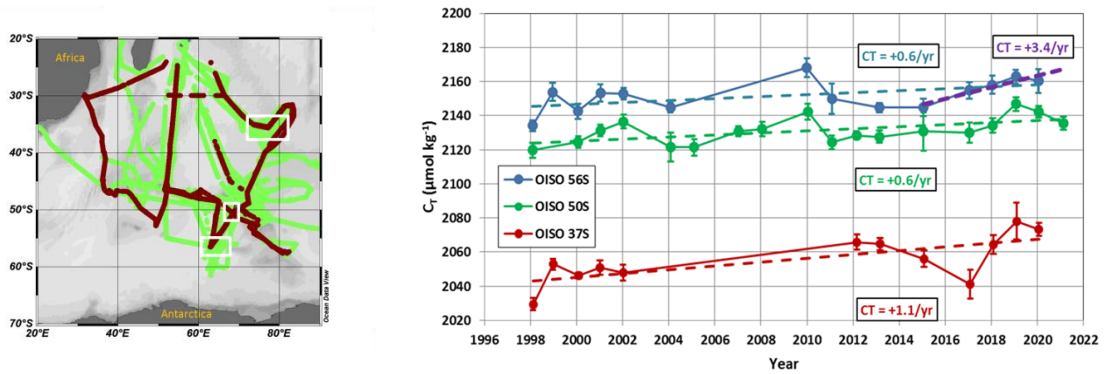


Figure 11: Left: Data in SNAPO-CO2-v1 dataset (green) and new data in version v2 (brown) in the South Western Indian Ocean (OISO cruises). Figure produced with ODV (Schlitzer, 2018). The white boxes identified the regions of data selected around 37°S, 50°S and 56°S for the trend analysis. Right: Time-series of average C_T concentrations in January-February at 37°S (red), 50°S (green) and 56°S (blue). The trends for each region are indicated (see also Table 6).

Table 6: Trend of C_T ($\mu\text{mol kg}^{-1} \text{yr}^{-1}$) and corresponding standard error in selected regions where data are available for more than 10 years. The projects/cruises for selection of the data in each domain are indicated.

Region	Period/Season	C_T trend ($\mu\text{mol kg}^{-1} \text{yr}^{-1}$)	Projects/Cruises
North Atlantic (NASPG)	1994-2023 April	+0.78 (0.23)	SURATLANT
North Atlantic (NASPG)	1994-2023 September	+1.09 (0.37)	SURATLANT
West. Trop. Atl. 5N-Eq	2009-2021 April-October	+3.31 (2.13)	AMAZOMIX, PIRATA-BR, TARA
West. Trop. Atl. Eq-10S	2005-2015, April-October	+3.05 (1.64)	CAMFIN-WAT, PIRATA-BR, VOS
Ligurian Sea 8E	1998-2022 Jan-Feb.	+0.94 (0.64)	ANTARES, DYFAMED, MOOSE-GE
Ligurian Sea 8E	1998-2023 July-August	+1.53 (0.46)	ANTARES, DYFAMED, MOOSE-GE
Subtropical Indian 37S	1998-2020 Jan-Feb.	+1.12 (0.36)	OISO
South West. Indian 50S	1998-2021 Jan-Feb.	+0.61 (0.21)	OISO
South West. Indian 56S	1998-2020 Jan-Feb.	+0.58 (0.27)	OISO
South West. Indian 56S	2015-2020 Jan-Feb.	+3.41 (0.73)	OISO
South East. Indian 60S	2002-2012 Jan-Feb.	+3.37 (0.94)	MINERVE, OISO
South East. Indian 60S	2002-2012 October	+4.79 (1.62)	MINERVE

824 5.5 The Coastal Zones

825

826 Coastal waters experience enhanced ocean acidification due to increasing CO_2 uptake, accumulation of
827 anthropogenic CO_2 (Bourgeois et al 2016; Laruelle et al, 2018; Roobaert et al, 2024a; Li et al, 2024) and from
828 local anthropogenic inputs through rivers or from air pollution (e.g. Sarma et al, 2015; Sridvi and Sarma, 2021;
829 Wimart-Rousseau et al, 2020). The changes of the CO_2 uptake in coastal zones are also linked to biological
830 processes (Mathis et al, 2024) or to circulation and local upwelling (Roobaert et al, 2024b), all controlling large
831 variability of A_T and C_T in space and time leading to uncertainties for detecting long-term changes of $p\text{CO}_2$ and
832 air-sea CO_2 fluxes in heterogeneous coastal waters (Dai et al 2022; Resplandy et al, 2024). At seasonal scale,
833 large differences between observations and models were also identified leading to differences in the coastal

834 ocean CO₂ sink up to 60% (Resplandy et al, 2024). It is thus important to document the seasonal cycles of A_T and
835 C_T to compare and correct models and thus to better predict future changes of biogeochemical properties in
836 coastal waters and their impact on marine ecosystems. A better understanding of the processes and their
837 retroaction in the coastal regions is also required regarding Marine Carbon Dioxide Removal (MCDR)
838 experiments and for their evaluation (e.g. Ho et al, 2023).

839 In the SNAPO-CO₂-v2 dataset new data have been added in the coastal zones at stations SOMLIT-
840 Brest, SOMLIT-Roscoff and SOMLIT-Point-B. They extend the period to 2022 or 2023 for temporal analysis.
841 New data in the French coastal zones have been also included from the COCORICO2 project documented in
842 detail by Petton et al (2024). The observations in coastal zones could be identified in the MARCATS regions
843 (Margins and CATchment Segmentation, Laruelle et al, 2013) (Figure 12) where little information is available
844 for quantifying the ocean CO₂ sink at the decadal scale and for evaluation of the anthropogenic CO₂ uptake
845 (Regnier et al, 2013; Dai et al, 2022; Li et al, 2024). To explore the change of the observed properties in the
846 coastal zones and have a flavor of the long-term C_T trends we selected the time series with at least 10 years of
847 data (Table 7, Figure 13). Except at high latitudes (Greenland and Antarctic coastal zones), we observed a
848 warming in coastal zones (Figure S11). Changes in salinity are also identified (increase or decrease) and results
849 of the trends are presented for salinity-normalized C_T at 34, 35 or 38 depending on the region. Although the
850 inter-annual variability is large in coastal waters, sometimes linked to extreme events (e.g. river discharges), we
851 observed an increase in $N-C_T$ at most of the 8 selected locations. The exceptions are the coastal zones in the Gulf
852 of Lion near the Rhone River and near Tasmania in October.

853 In the Gulf of Lion, the new data in the coastal zone confirmed the first view at the SOLEMIO station
854 over 2016-2018 (Bay of Marseille, Wimart-Rousseau et al, 2020). In this region the lowest C_T was observed in
855 summer 2022 (average C_T of $2238.6 \pm 21.0 \mu\text{mol kg}^{-1}$), much lower than in 2015 ($2290.8 \pm 44.7 \mu\text{mol kg}^{-1}$). Over
856 the continental shelf south of Tasmania (MARCATS #34), the trend in $N-C_T$ was positive in summer but not
857 significant in October. In October this was associated with an increase in Salinity and in A_T probably linked to
858 advective processes via the reversal and variability of the Zeehan or the East Australian currents. From our data a
859 warming of $+0.06^\circ\text{C yr}^{-1}$ was identified for both seasons over 2002-2012 as previously observed south of
860 Tasmania over 1991-2003 impacting the $p\text{CO}_2$ trend and air-sea CO₂ fluxes in this region (Borges et al, 2008).
861 The difference in the $N-C_T$ trends in austral summer and spring calls for new detailed studies with extended data
862 in this region. At high latitude in the Adélie Land (Antarctic coast MARCATS #45), the variability of $N-C_T$ was
863 large (range from 2150 to 2200 $\mu\text{mol kg}^{-1}$, Figure 13) and the trend over 10 years in summer was not significant
864 (Table 7). As opposed to the open zone at 60°S (Figure 10) the C_T concentrations in the coastal zone near
865 Antarctica were not increasing, probably linked to competitive processes between anthropogenic uptake, changes
866 in primary production, mixing or ice melting (Shadwick et al, 2013, 2014). More data are needed to better
867 evaluate the changes of the carbonate system in Antarctic coastal zones where bottom waters are formed and
868 transport anthropogenic CO₂ at lower latitudes (Zhang et al, 2023).

869 For the coastal time series SOMLIT where annual trends could be estimated (sampling at monthly
870 resolution), the $N-C_T$ increase ($+2.1$ to $3.4 \mu\text{mol kg}^{-1} \text{ yr}^{-1}$) is close or higher than the anthropogenic signal leading
871 to a decrease in pH ranging between -0.05 to $-0.06 \text{ TS decade}^{-1}$. The new data added in the SNAPO-CO₂-v2
872 dataset (2016-2023) confirm the progressive increase in C_T and the acidification in the western Mediterranean
873 Sea and in the North-East Atlantic coastal zones (Kapsenberg et al, 2017; Gac et al, 2021).

874
875
876
877
878
879
880
881
882
883
884
885
886
887
888
889
890
891
892
893
894
895
896
897
898
899
900
901
902
903
904
905
906
907
908
909
910
911
912
913
914
915
916
917
918
919
920
921
922
923
924
925
926
927
928
929
930
931
932
933

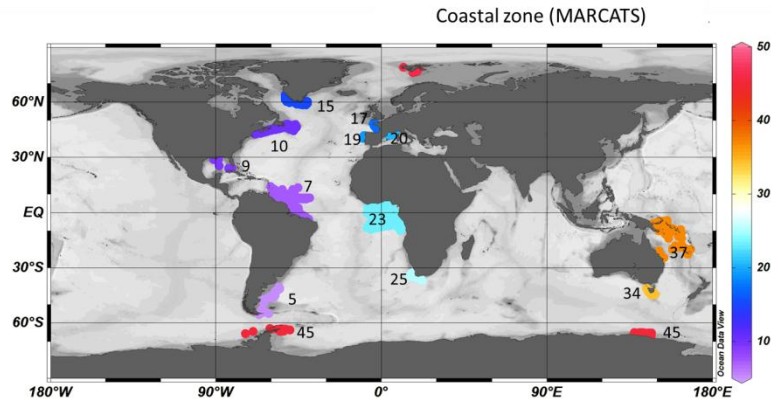


Figure 12: Location of A_T and C_T data available in the coastal zones in the SNAPO-CO2-v2 dataset. Numbers and Color code identify MARCATS region (Laruelle et al, 2013). Figure produced with ODV (Schlitzer, 2018).

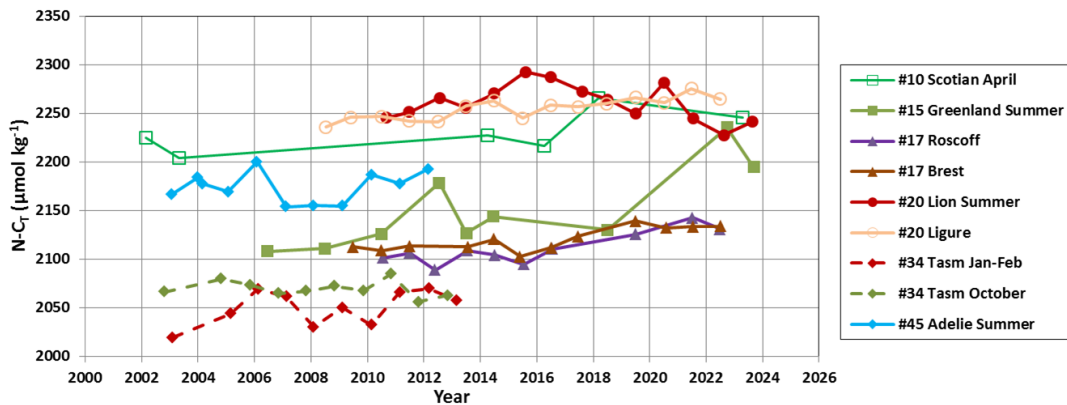


Figure 13: Time-series of average $N-C_T$ concentrations ($\mu\text{mol kg}^{-1}$) in selected MARCATS regions for different period when data are available for ten years or more. The trends and periods for each region are indicated in Table 7.

Table 7: Trends of $N-C_T$ ($\mu\text{mol kg}^{-1} \text{ yr}^{-1}$) and corresponding standard errors in selected coastal regions where data are available for 10 years or more. The projects/cruises for selection of the data in each domain are indicated. MARCATS # regions also identified. Salinity values used for C_T normalization are indicated.

Region #MARCATS	Period	Season	$N-C_T$ Trend ($\mu\text{mol kg}^{-1} \text{ yr}^{-1}$)	Salinity	Projects/Cruises
Scotian #10	2002-2023	March-April	+1.71 (0.97)	35	SURATLANT
Greenland #15	2006-2023	June-mid-Sept	+5.77 (1.62)	35	OVIDE, SURATLANT
Roscoff #17	2010-2022	All season	+3.40 (0.76)	35	CHANNEL, COCORICO2, SOMLIT ROSCOFF
Bay of Brest #17	2009-2022	All seasons	+2.17 (0.52)	35	SOMLIT-Brest, COCORICO2, ECOSCOPIA,
LION#20	2010-2023	June-Sept	-1.19 (1.25)	38	COCORICO2, MOOSE-GE, SOLEMIO (a)
LIGURE#20	2008-2022	All seasons	+2.12 (0.36)	38	SOMLIT-Point-B, MOOSE-GE
Tasmania #34	2003-2013	Jan-Feb	+2.73 (1.72)	35	MINERVE, OISO
Tasmania #34	2002-2012	Oct	-0.65 (0.89)	35	MINERVE, OISO
Adélie #45	2002-2012	Dec-Feb	+0.63 (0.70)	34	MINERVE, OISO

(a) For LION, some data in summer were also used from punctual cruises: AMOR-BFlux, CARBORHONE, DICASE, LATEX, MESURHOBENT, MISSRHODIA2 and MOLA.

934 6 Summary and suggestions

935

936 This work extends in time and in new oceanic regions the A_T and C_T data presented in the first SNAPO-
937 CO₂ synthesis (Metzl et al, 2024a). It includes now more than 67 000 surface and water column observations in
938 all oceanic basins, in the Mediterranean Sea, in the coastal zones, near coral reefs, and in rivers. The data
939 synthesized in version v2 are based on measurements of A_T and C_T performed between 1993 and 2023 with an
940 accuracy of $\pm 4 \mu\text{mol kg}^{-1}$. Based on a secondary quality control, 91% of the A_T and C_T data are considered as
941 good (WOCE Flag 2) and 6% probably good (Flag 3). For the open ocean this synthesis complements the
942 SOCAT, GLODAP and SPOTS data products (Bakker et al., 2016; Lauvset et al., 2024; Lange et al, 2024). For
943 the coastal sites this also complements the synthesis of coastal time-series in the Iberian Peninsula (Padin et al,
944 2020), in the Canadian Atlantic continental shelf (Gibb et al, 2023) and around North America (Fassbender et al.,
945 2018; Jiang et al., 2021; Jiang et al 2024, in prep). The SNAPO-CO₂ dataset enables to investigate the seasonal
946 cycles, the inter-annual variability and the decadal trends of A_T and C_T in various oceanic provinces. The same
947 temporal analyses could be investigated for other carbonate system properties such as $f\text{CO}_2$ or pH calculated
948 from A_T and C_T for air-sea CO₂ flux estimates or ocean acidification studies (Figure 14).

949

950

951

952

953

954

955

956

957

958

959

960

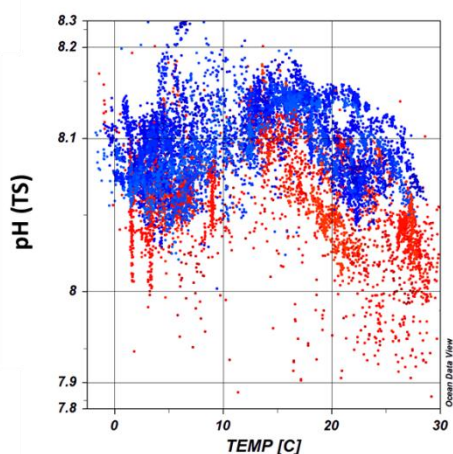
961

962

963

964

965



966 **Figure 14:** An example of observed ocean acidification derived from the SNAPO-CO₂-v2 dataset: pH (TS)
967 calculated with A_T and C_T data are presented as a function of temperature (°C) for years 1998-2002 (blue
968 symbols) and 2020-2023 (red symbols) and for salinity > 33 (Nb data selected with flag 2 = 11994). In recent
969 years the pH was lower. Figure produced with ODV (Schlitzer, 2018).
970

971 In almost all regions the new data in 2021-2023 indicated that the C_T concentrations were higher in
972 recent years. In regions where data are available for more than 2 decades, the time-series show an increase of sea
973 surface C_T (North Atlantic, Southern Indian Ocean and Ligurian Sea) with a rate close to or higher than the
974 changes expected from anthropogenic CO₂ uptake. It is also recognized that at seasonal scale the C_T trends could
975 be different. However, with the data in hand, the long-term trend of C_T cannot be quantified with confidence to
976 compare with the anthropogenic carbon uptake in some regions. This is the case in the eastern tropical Atlantic
977 subject to high inter-annual variability (Lefèvre et al., 2021, 2024) although new data have been added over
978 2005-2022 in this region (Table 1, Figure S9). When data are available for less than a decade the increase in C_T
979 was observed but the trend was uncertain due to large inter-annual variability (e.g. Adélie Land). An exception
980 was identified in the coastal zone in the Gulf of Lion (Mediterranean Sea) where summer data since 2010 present

981 a decrease in C_T most pronounced since 2015 (C_T trend = $-5.2 \pm 1.5 \mu\text{mol kg}^{-1} \text{yr}^{-1}$). Such C_T decrease over 10
982 years was also observed at the Hawaii Ocean Time series, HOT over 2010-2020 (Dore et al, 2009,
983 <https://hahana.soest.hawaii.edu/hot/hotco2/hotco2.html>, last access: 27 August 2024).

984 Although the A_T concentrations present significant inter-annual variability such as in the NASPG, in the
985 Topical Atlantic or the Adélie land and coastal zones, A_T appears relatively constant over time except at these
986 locations. In the open ocean, we observed an increase of A_T in the Southern Ocean south of the Polar Front
987 around 60°S in 2003-2012 not directly linked to salinity. In the coastal zones a decrease of A_T was pronounced
988 south of Greenland. In the coast in the Gulf of Lion, as observed for C_T , A_T decreased (A_T trend = $-2.8 \pm 1.2 \mu\text{mol}$
989 $\text{kg}^{-1} \text{yr}^{-1}$). This is opposed to the changes observed in the Ligurian Sea at station SOMLIT-Point-B, where C_T and
990 A_T increased over 2007-2015 (Kapsenberg et al, 2017) highlighting the contrasting C_T and A_T trends in the
991 Mediterranean coastal zones where ocean acidification is detected (here over 2008-2022, pH trend of -0.048
992 $\pm 0.003 \text{decade}^{-1}$). With the continuous warming, reduced stratification and the rapid pH change observed in the
993 Mediterranean Sea, how the marine ecosystems will respond in the future should be addressed (e.g. Howes et al,
994 2015; Maugendre et al 2015; Lacoue-Labarthe et al, 2016). The SNAPO-CO2-v2 dataset could also be used to
995 explore and analyze the changes of the carbonate system occurring during extreme events such as marine heat
996 waves, rapid freshening, deep convection or high phytoplankton bloom events.

997 This dataset could also serve for validating autonomous platforms capable of measuring pH and $f\text{CO}_2$
998 properties (Sarmiento et al, 2023) and, along with other synthesis products (Jiang et al, 2024 in prep.), provides
999 an additional reference dataset for the development and validation of regional biogeochemical models for
1000 simulating air-sea CO_2 fluxes. Thanks to the RECCAP2 stories, it has been recognized that Ocean
1001 Biogeochemical Models present biases in the seasonal cycle of C_T and A_T due to inadequate representation of
1002 biogeochemical cycles (e.g. Hauck et al, 2023; Rodgers et al, 2023; Sarma et al, 2023; Pérez et al, 2024;
1003 Resplandy et al, 2024). The SNAPO-CO2-v2 dataset could be used to guide analyses for regional or global
1004 biogeochemical models for A_T and C_T comparison and validation from seasonal to decadal scales. Our dataset is
1005 also essential for training and validating neural networks capable of predicting variables in the carbonate system
1006 (e.g. Fourier et al, 2020; Chau et al, 2024a; Gregor et al, 2024), thereby enhancing observations of marine CO_2 at
1007 different spatial and temporal scales. Furthermore, we encourage the use of this dataset (or part of it), at sea or
1008 prior going to sea for cruise planning. Indeed, using the approach of Davis and Goyet (2021) which takes into
1009 account the multiple constraints (ship-time, number of samples, etc.), it is possible to determine the most
1010 appropriate sampling strategy (Guglielmi et al., 2022, 2023), to reach the specific scientific objectives of each
1011 cruise.

1012 The data presented here are available online on the Seano server (<https://doi.org/10.17882/102337>) in a
1013 file identifying version v1 and v2. The sources of the original datasets (doi) with the associated references are
1014 listed in the Supplementary Material (Tables S3, S4). As for version v1 we invite the users to comment on any
1015 anomaly that would have not been detected or to suggest potential misqualification of data in the present product
1016 (e.g. data probably good although assigned with flag 3, probably wrong). As for SOCAT or GLODAP, we
1017 expect to update the SNAPO-CO2 dataset once new observations are obtained and controlled.

1018
1019 **7 Data availability**

1020 Data presented in this study are available at Seanoe (Metzl et al, 2024d, <https://www.seanoe.org>,
1021 <https://doi.org/10.17882/102337>. See also <https://doi.org/10.17882/95414> for version V1. The dataset is also
1022 available at <https://explore.webodv.awi.de/ocean/carbon/snapo-co2/>

1023
1024 *Author contributions.* NM prepared the data synthesis, the figures and wrote the draft of the manuscript with
1025 contributions from all authors. JF measured the discrete samples since 2014, with the help from CM and CLM,
1026 and prepared the individual reports for each project. NM and JF pre-qualified the discrete A_T/C_T data. CLM and
1027 NM are co-Is of the ongoing OISO project and qualified the underway A_T/C_T data from OISO cruises. FT and
1028 CG were PIs of the MINERVE cruises. All authors have contributed either to organizing cruises, sample
1029 collection and/or data qualification, and reviewed the manuscript.

1030
1031 *Competing interest.* The authors have the following competing interests: At least one of the (co-)authors is a
1032 member of the editorial board of Earth System Science Data

1033
1034 *Acknowledgments.* Most of the A_T and C_T data presented in this study were measured at the SNAPO-CO2 facility
1035 (Service National d'Analyse des Paramètres Océaniques du CO2) housed by the LOCEAN laboratory and part of
1036 the OSU ECCE Terra at Sorbonne University and INSU/CNRS analytical services. Support by INSU/CNRS, by
1037 OSU ECCE Terra and by LOCEAN, is gratefully acknowledged as well as support by different French "Services
1038 nationaux d'Observations", such as OISO/CARAUS, SOMLIT, PIRATA, SSS and MOOSE. We thank the
1039 research infrastructure ICOS (Integrated Carbon Observation System) France for funding a large part of the
1040 analyses. We thank the IRD (Institut de Recherche pour le Développement) and the French-Brazilian IRD-
1041 FAPEMA program for funding observations in the tropical Atlantic. We thank the French oceanographic fleet
1042 ("Flotte océanographique française") for financial and logistic support for most cruises listed in this synthesis
1043 and for the OISO program (<https://campagnes.flotteoceanographique.fr/series/228/>). We acknowledge the
1044 MOOSE program (Mediterranean Ocean Observing System for the Environment,
1045 <https://campagnes.flotteoceanographique.fr/series/235/fr/>) coordinated by CNRS-INSU and the Research
1046 Infrastructure ILICO (CNRS-IFREMER). The CocoriCO2 project was founded by European Maritime and
1047 Fisheries Fund (grant no. 344, 2020–2023) and benefited from a subsidy from the Adour-Garonne water agency.
1048 We thank the following programs coordinated by A. Tribollet which have contributed to the acquisition of the
1049 data in Mayotte: CARBODISS funded by CNRS-INSU in 2018-2019, Future Maore reefs funded by Next
1050 Generation UE-France Relance in 2021-2023, and OA-ME funded by a Belmont Forum International (ANR) in
1051 2020-2026. We thank the program Mermex-Mistrals CNRS for supporting AMOR-BFlux, CARBORHONE,
1052 DICASE and MESURHOBENT cruises and the program EC2CO-INSU for supporting MISSRHODIA2 cruise.
1053 The ACCESS project was supported by CNRS MISTRALS and the DELTARHONE-1 by EC2CO-INSU. The
1054 ACIDHYPO project was founded by CNRS International Emerging Actions; we thank Captain and crew of the
1055 R/V Savannah from the Skidaway Institute of Oceanography (University of Georgia) for their support and
1056 technical assistance during the operations at sea. The AMAZOMIX project was funded by French
1057 Oceanographic Fleet, INSU (LEFE), IRD (LMI TAPICOA), CNES (TOSCA MIAMAZ project) and by the
1058 French-Brazilian international program GUYAMAZON. The OISO program was supported by the French
1059 institutes INSU (Institut National des Sciences de l'Univers) and IPEV (Institut Polaire Paul-Emile Victor), OSU

1060 Ecce-Terra (at Sorbonne Université), and the French program SOERE/Great-Gases. We also thank the Research
1061 Infrastructure ILICO (<https://www.ir-ilico.fr>). We warmly thank Alain Poisson who initiated the MINERVE
1062 program and performed many of the measurements onboard R/V Astrolabe from 2002 through 2018. We thank
1063 all colleagues and students who participated to the cruises and have carefully collected the precious seawater
1064 samples. We thank Frédéric Merceur (IFREMER) for preparing the page and data availability on Seanoe and
1065 Reiner Schlitzer (AWI) for including the SNAPO-CO2 dataset in the ODV portal. We thank the associated editor
1066 Sebastiaan van de Velde to manage this manuscript, and Kim Currie and Toste Tanhua for their suggestions that
1067 helped to improve this article.

1068

1069 **References:**

1070

1071 Ait Ballagh, F.E., Rabouille, C., Andrieux-Loyer, F. et al. Spatial Variability of Organic Matter and Phosphorus
1072 Cycling in Rhône River Prodelta Sediments (NW Mediterranean Sea, France): a Model-Data Approach.
1073 *Estuaries and Coasts* 44, 1765–1789, <https://doi.org/10.1007/s12237-020-00889-9>, 2021

1074

1075 Álvarez, M., Catalá, T. S., Civitarese, G., Coppola, L., Hassoun, A. E.R., Ibello, V., Lazzari, P., Lefevre, D.,
1076 Macías, D., Santinelli, C. and Ulses, C.: Chapter 11 - Mediterranean Sea general biogeochemistry, Editor(s):
1077 Katrin Schroeder, Jacopo Chiggiato, *Oceanography of the Mediterranean Sea*, Elsevier, Pages 387-451,
1078 <https://doi.org/10.1016/B978-0-12-823692-5.00004-2>, 2023.

1079

1080 Bakker, D. C. E., Pfeil, B., Landa, C. S., Metzl, N., O'Brien, K. M., Olsen, A., Smith, K., Cosca, C., Harasawa,
1081 S., Jones, S. D., Nakaoka, S.-I., Nojiri, Y., Schuster, U., Steinhoff, T., Sweeney, C., Takahashi, T., Tilbrook, B.,
1082 Wada, C., Wanninkhof, R., Alin, S. R., Balestrini, C. F., Barbero, L., Bates, N. R., Bianchi, A. A., Bonou, F.,
1083 Boutin, J., Bozec, Y., Burger, E. F., Cai, W.-J., Castle, R. D., Chen, L., Chierici, M., Currie, K., Evans, W.,
1084 Featherstone, C., Feely, R. A., Fransson, A., Goyet, C., Greenwood, N., Gregor, L., Hankin, S., Hardman-
1085 Mountford, N. J., Harlay, J., Hauck, J., Hoppema, M., Humphreys, M. P., Hunt, C. W., Huss, B., Ibáñez, J. S.
1086 P., Johannessen, T., Keeling, R., Kitidis, V., Körtzinger, A., Kozyr, A., Krasakopoulou, E., Kuwata, A.,
1087 Landschützer, P., Lauvset, S. K., Lefèvre, N., Lo Monaco, C., Manke, A., Mathis, J. T., Merlivat, L., Millero, F.
1088 J., Monteiro, P. M. S., Munro, D. R., Murata, A., Newberger, T., Omar, A. M., Ono, T., Paterson, K., Pearce, D.,
1089 Pierrot, D., Robbins, L. L., Saito, S., Salisbury, J., Schlitzer, R., Schneider, B., Schweitzer, R., Sieger, R.,
1090 Skjelvan, I., Sullivan, K. F., Sutherland, S. C., Sutton, A. J., Tadokoro, K., Telszewski, M., Tuma, M., Van
1091 Heuven, S. M. A. C., Vandemark, D., Ward, B., Watson, A. J., and Xu, S.: A multi-decade record of high-quality
1092 fCO₂ data in version 3 of the Surface Ocean CO₂ Atlas (SOCAT), *Earth Syst. Sci. Data*, 8, 383-413,
1093 doi:10.5194/essd-8-383-2016. 2016.

1094

1095 Barral, Q-B., Zakardjian, B. Dumas, F., Garreau, P., Testor, P., and Beuvier, J.: Characterization of fronts in the
1096 Western Mediterranean with a special focus on the North Balearic Front, *Progress in Oceanography*, Volume
1097 197, 102636, <https://doi.org/10.1016/j.pocean.2021.102636>. 2021

1098

1099 Barré, L., Diaz, F., Wagener, T., Van Wambeke, F., Mazoyer, C., Yohia, C., and Pinazo, C.: Implementation and
1100 assessment of a model including mixotrophs and the carbonate cycle (Eco3M_MIX-CarbOx v1.0) in a highly
1101 dynamic Mediterranean coastal environment (Bay of Marseille, France) – Part 1: Evolution of ecosystem
1102 composition under limited light and nutrient conditions, *Geosci. Model Dev.*, 16, 6701–6739,
1103 <https://doi.org/10.5194/gmd-16-6701-2023>, 2023.

1104

1105 Barré, L., Diaz, F., Wagener, T., Mazoyer, C., Yohia, C., and Pinazo, C.: Implementation and assessment of a
1106 model including mixotrophs and the carbonate cycle (Eco3M_MIX-CarbOx v1.0) in a highly dynamic
1107 Mediterranean coastal environment (Bay of Marseille, France) – Part 2: Towards a better representation of total
1108 alkalinity when modeling the carbonate system and air–sea CO₂ fluxes, *Geosci. Model Dev.*, 17, 5851–5882,
1109 <https://doi.org/10.5194/gmd-17-5851-2024>, 2024.

1110

1111 BERTRAND Arnaud, DE SAINT LEGER Emmanuel, KOCH-LARROUY Ariane : AMAZOMIX 2021 cruise,
1112 RV Antea, <https://doi.org/10.17600/18001364>, 2021

1113
1114 Bittig, H.C., Steinhoff, T., Claustre, H., Fiedler, B., Williams, N.L., Sauzède, R., Körtzinger, A. and Gattuso, J.-
1115 P.: An Alternative to Static Climatologies: Robust Estimation of Open Ocean CO₂ Variables and Nutrient
1116 Concentrations From T, S, and O₂ Data Using Bayesian Neural Networks. *Front. Mar. Sci.* 5:328. doi:
1117 10.3389/fmars.2018.00328, 2018
1118
1119 Bonou, F.K., Noriega, C., Lefèvre, N., Araujo, M.: Distribution of CO₂ parameters in the Western Tropical
1120 Atlantic Ocean, *Dynamics of Atmospheres and Oceans*, 73: 47-60
1121 <http://dx.doi.org/10.1016/j.dynatmoce.2015.12.001>, 2016
1122
1123 Bonou, F., Medeiros, C., Noriega, C., Araujo, M., Aubains Hounsou-Gbo, A., and Lefèvre N. : A comparative
1124 study of total alkalinity and total inorganic carbon near tropical Atlantic coastal regions. *J Coast Conserv* 26, 31,
1125 <https://doi.org/10.1007/s11852-022-00872-5>, 2022
1126
1127 Borges A.V., B. Tilbrook, N. Metzl, A. Lenton and B. Delille: Inter-annual variability of the carbon dioxide
1128 oceanic sink south of Tasmania, *Biogeosciences*, 5, 141-155. <https://doi.org/10.5194/bg-5-141-2008>, 2008
1129
1130 Bourgeois, T., J. C. Orr, L. Resplandy, J. Terhaar, C. Ethé, M. Gehlen, and L. Bopp: Coastal-ocean uptake of
1131 anthropogenic carbon. *Biogeosciences*, 13, 4167-4185, doi: 10.5194/bg-13-4167-2016., 2016
1132
1133 BOURLES Bernard (1997) PIRATA, <https://doi.org/10.18142/14>
1134
1135 BOURLES Bernard (2019) PIRATA FR29 cruise, RV Thalassa, <https://doi.org/10.17600/18000875>
1136
1137 BOURLES Bernard, LLIDO Jérôme (2020) PIRATA FR30 cruise, RV Thalassa,
1138 <https://doi.org/10.17600/18000690>
1139
1140 BOURLES Bernard, LLIDO Jérôme (2022) PIRATA FR32 cruise, RV Thalassa,
1141 <https://doi.org/10.17600/18001832>
1142
1143 Bozec Y., Cariou, T., Mace, E., Morin, P., Thuillier, D., Vernet, M.: Seasonal dynamics of air-sea CO₂ fluxes in
1144 the inner and outer Loire estuary (NW Europe). *Estuarine Coastal And Shelf Science*, 100, 58-71.
1145 <https://doi.org/10.1016/j.ecss.2011.05.015>, 2012
1146
1147 BOZEC Yann (2009) CO₂ARVOR 3 cruise, RV Côtes De La Manche, <https://doi.org/10.17600/9480170>
1148
1149 BOZEC Yann (2009) CO₂ARVOR 2 cruise, RV Côtes De La Manche, <https://doi.org/10.17600/9480110>
1150
1151 BOZEC Yann (2009) CO₂ARVOR 1 cruise, RV Thalia, <https://doi.org/10.17600/9070070>
1152
1153 Brandon, M., C. Goyet, F. Touratier, N. Lefèvre, E. Kestenare, and R. Morrow : Spatial and temporal variability
1154 of the physical, carbonate and CO₂ properties in the Southern Ocean surface waters during austral summer
1155 (2005-2019). *Deep Sea Res. Part I*, 187, 103836, <https://doi.org/10.1016/j.dsr.2022.103836>. 2022
1156
1157 Broullón, D., Pérez, F. F., Velo, A., Hoppema, M., Olsen, A., Takahashi, T., Key, R. M., Tanhua, T., González-
1158 Dávila, M., Jeansson, E., Kozyr, A., and van Heuven, S. M. A. C.: A global monthly climatology of total
1159 alkalinity: a neural network approach, *Earth Syst. Sci. Data*, 11, 1109–1127, [https://doi.org/10.5194/essd-11-](https://doi.org/10.5194/essd-11-1109-2019)
1160 1109-2019. 2019
1161
1162 Broullón, D., Pérez, F. F., Velo, A., Hoppema, M., Olsen, A., Takahashi, T., Key, R. M., Tanhua, T., Santana-
1163 Casiano, J. M., and Kozyr, A.: A global monthly climatology of oceanic total dissolved inorganic carbon: a

1164 neural network approach, *Earth Syst. Sci. Data*, 12, 1725–1743, <https://doi.org/10.5194/essd-12-1725-2020>.
1165 2020
1166
1167 CARIOU Thierry, BOZEC Yann (2010) CO2ARVOR 4 cruise, RV Thalia, <https://doi.org/10.17600/10070040>
1168
1169 Carter, B. R., Feely, R. A., Williams, N. L., Dickson, A. G., Fong, M. B., and Takeshita, Y.: Updated methods
1170 for global locally interpolated estimation of alkalinity, pH, and nitrate. *Limnology and Oceanography: Methods*,
1171 16: 119-131. doi: 10.1002/lom3.10232, 2018
1172
1173 Chau, T.-T.-T., Gehlen, M., Metzl, N., and Chevallier, F.: CMEMS-LSCE: a global, 0.25°, monthly
1174 reconstruction of the surface ocean carbonate system, *Earth Syst. Sci. Data*, 16, 121–160,
1175 <https://doi.org/10.5194/essd-16-121-2024>, 2024a.
1176
1177 Chau, T.-T.-T., Chevallier, F., and Gehlen, M.: Global analysis of surface ocean CO₂ fugacity and air-sea fluxes
1178 with low latency. *Geophysical Research Letters*, 51, e2023GL106670. <https://doi.org/10.1029/2023GL106670>,
1179 2024b
1180
1181 Cheng, L. J., Abraham, J., Zhu, J., Trenberth, K. E., Fasullo, J., Boyer, T., Locarnini, R., Zhang, B., Yu, F. J.,
1182 Wan, L. Y., Chen, X. R., Song, X. Z., Liu, Y. L., and Mann, M. E.: Record-setting ocean warmth continued in
1183 2019, *Adv. Atmos. Sci*, 37, 137-142. <https://doi.org/10.1007/s00376-020-9283-7>, 2020
1184
1185 Cheng, L., Abraham, J., Trenberth, K.E. et al. New Record Ocean Temperatures and Related Climate Indicators
1186 in 2023. *Adv. Atmos. Sci.*, <https://doi.org/10.1007/s00376-024-3378-5>, 2024
1187
1188 Conan, P., Guieux, A., and Vuillemin, R.: MOOSE (MOLA), <https://doi.org/10.18142/234>, 2020.
1189
1190 Copin-Montégut, C.: Alkalinity and carbon budgets in the Mediterranean Sea, *Global Biogeochemical Cycles*,
1191 vol. 7, pp. 915–925, 1993.
1192
1193 Coppola, L., and Diamond-Riquier, E.: MOOSE (DYFAMED), <https://doi.org/10.18142/131>, 2008.
1194
1195 Coppola Laurent, Diamond Riquier Emilie, Carval Thierry, Irisson Jean-Olivier, Desnos Corinne: Dyfamed
1196 observatory data. SEANOE. <https://doi.org/10.17882/43749>, 2024
1197
1198 Coppola, L., Fourier, M., Pasqueron de Fommervault, O., Poteau, A., Riquier, E. D. and Béquery, L.:
1199 Highresolution study of the air-sea CO₂ flux and net community oxygen production in the Ligurian Sea by a
1200 fleet of gliders. *Front. Mar. Sci.* 10:1233845. doi: 10.3389/fmars.2023.1233845, 2023
1201
1202 Curbelo-Hernández, D., Pérez, F. F., González-Dávila, M., Gladyshev, S. V., González, A. G., González-
1203 Santana, D., Velo, A., Sokov, A., and Santana-Casiano, J. M.: Ocean Acidification trends and Carbonate System
1204 dynamics in the North Atlantic Subpolar Gyre during 2009–2019, *EGUsphere* [preprint],
1205 <https://doi.org/10.5194/egusphere-2024-1388>, 2024.
1206
1207 Currie, K. I., Reid, M. R., and Hunter, K. A.: Interannual variability of carbon dioxide draw-down by
1208 subantarctic surface water near New Zealand, *Biogeochemistry*, 104, 23–34, [https://doi.org/10.1007/s10533-009-](https://doi.org/10.1007/s10533-009-9355-3)
1209 9355-3, 2011.
1210
1211 Cyronak, T., Santos, I. R., Erler, D. V., and Eyre, B. D.: Groundwater and porewater as major sources of
1212 alkalinity to a fringing coral reef lagoon (Muri Lagoon, Cook Islands), *Biogeosciences*, 10, 2467–2480,
1213 <https://doi.org/10.5194/bg-10-2467-2013>, 2013.
1214
1215 Dai, M., J. Su, Y. Zhao, E. E. Hofmann, Z. Cao, W. –J. Cai, J. Gan, F. Lacroix, G. G. Laruelle, F. Meng, J. D.
1216 Müller, P. A.G. Regnier, G. Wang, Z. Wang, 2022. Carbon Fluxes in the Coastal Ocean: Synthesis, *Boundary*

1217 Processes and Future Trends, *Annual Review of Earth and Planetary Sciences*, 50:1, 593-626,
1218 <https://doi.org/10.1146/annurev-earth-032320-090746>, 2022
1219
1220 Davis D. and Goyet, C.: Balanced Error Sampling with applications to ocean biogeochemical sampling.
1221 Collection études, Presses Universitaires de Perpignan, 224p. ISBN : 978-2-35412-452-6, 2021
1222
1223 Dickson, A. G., Sabine, C. L., and Christian, J. R.: Guide to best practices for ocean CO₂ measurements, North
1224 Pacific Marine Science Organization, Sidney, British Columbia, 191, <https://doi.org/10.25607/OBP-1342>, 2007.
1225
1226 DOE: Handbook of Methods for Analysis of the Various Parameters of the Carbon Dioxide System in Seawater;
1227 version 2, A.G. Dickson et C. Goyet, eds, ORNL/CDIAC-74, <https://doi.org/10.2172/10107773>, 1994.
1228
1229 Doney, S. C., Fabry, V. J., Feely, R. A., and Kleypas, J. A., Ocean acidification: The other CO₂ problem. *Annual*
1230 *Review of Marine Science*, 1(1), 169–192. 10.1146/annurev.marine.010908.163834, 2009
1231
1232 Doney, S. C., Busch, D. S., Cooley, S. R., and Kroeker, K. J.: The Impacts of Ocean Acidification on Marine
1233 Ecosystems and Reliant Human Communities. *Annual Review of Environment and Resources* 45:1,
1234 <https://doi.org/10.1146/annurev-environ-012320-083019>. 2020
1235
1236 Dumoulin J-P, Pozzato L., Rassman J., Toussaint F., Fontugne M., Tisnerat-Laborde N., Beck L., Caffy I.,
1237 Delque-Kolic E., Moreau C., Rabouille C. : Isotopic Signature (13C, 14C) of DIC in Sediment Pore Waters: An
1238 Example from the Rhone River Delta. *Radiocarbon*, 60(5), 1465-1481. <https://doi.org/10.1017/RDC.2018.111>,
1239 2018.
1240
1241 Dumoulin J-P, Rabouille C, Pourtout S, Bombled B, Lansard B, Caffy I, Hain S, Perron M, Sieudat M, Thellier
1242 B, Delqué-Koli E, Moreau C, Beck L (2022). : Identification in Pore Waters of Recycled Sediment Organic
1243 Matter Using the Dual Isotopic Composition of Carbon (13C and 14C): New Data From the Continental Shelf
1244 Influenced by the Rhône River. *Radiocarbon*, 64(6), 1617-1627. <https://doi.org/10.1017/RDC.2022.71>, 2022.
1245
1246 Edmond, J. M.: High precision determination of titration alkalinity and total carbon dioxide content of sea water
1247 by potentiometric titration, *Deep-Sea Res.*, 17, 737–750, [https://doi.org/10.1016/0011-7471\(70\)90038-0](https://doi.org/10.1016/0011-7471(70)90038-0), 1970.
1248
1249 Eyring, V., Righi, M., Lauer, A., Evaldsson, M., Wenzel, S., Jones, C., Anav, A., Andrews, O., Cionni, I., Davin,
1250 E. L., Deser, C., Ehbrecht, C., Friedlingstein, P., Gleckler, P., Gottschaldt, K.-D., Hagemann, S., Juckes, M.,
1251 Kindermann, S., Krasting, J., Kunert, D., Levine, R., Loew, A., Mäkelä, J., Martin, G., Mason, E., Phillips, A. S.,
1252 Read, S., Rio, C., Roehrig, R., Senfleben, D., Sterl, A., van Ulf, L. H., Walton, J., Wang, S., and Williams, K.
1253 D.: ESMValTool (v1.0) – a community diagnostic and performance metrics tool for routine evaluation of Earth
1254 system models in CMIP, *Geosci. Model Dev.*, 9, 1747-1802, doi:10.5194/gmd-9-1747-2016, 2016.
1255
1256 Fabry, V. J., Seibel, B. A., Feely, R. A. and Orr, J. C.: Impacts of ocean acidification on marine fauna and
1257 ecosystem processes. *ICES J. Mar. Sci.* 65, 414–432. <https://doi.org/10.1093/icesjms/fsn048>, 2008.
1258
1259 Faranda, D., Pascale, S., Bulut, B.: Persistent anticyclonic conditions and climate change exacerbated the
1260 exceptional 2022 European-Mediterranean drought. *Environ. Res. Lett.*, 18, 034030, DOI 10.1088/1748-
1261 9326/acbc37, 2023
1262
1263 Fassbender, A. J., Alin, S. R., Feely, R. A., Sutton, A. J., Newton, J. A., Krembs, C., Bos, J., Keyzers, M., Devol,
1264 A., Ruef, W., and Pelletier, G.: Seasonal carbonate chemistry variability in marine surface waters of the US
1265 Pacific Northwest, *Earth Syst. Sci. Data*, 10, 1367–1401, <https://doi.org/10.5194/essd-10-1367-2018>, 2018.
1266
1267 Fay, A. R., and McKinley, G. A.: Global open-ocean biomes: Mean and temporal variability. *Earth System*
1268 *Science Data*, 6(2), 273–284. <https://doi.org/10.5194/essd-6-273-2014>, 2014

1269
1270 Fourrier, M., Coppola, L., Claustre, H., D'Ortenzio, F., Sauzède, R. and Gattuso, J.-P.: A regional neural
1271 network approach to estimate water-column nutrient concentrations and carbonate system variables in the
1272 Mediterranean Sea: CANYON-MED. *Frontiers in Marine Science*, 7:620,
1273 <https://www.frontiersin.org/articles/10.3389/fmars.2020.00620>, 2020.
1274
1275 Friedlingstein, P., O'Sullivan, M., Jones, M. W., Andrew, R. M., Gregor, L., Hauck, J., Le Quéré, C., Luijkx, I.
1276 T., Olsen, A., Peters, G. P., Peters, W., Pongratz, J., Schwingshackl, C., Sitch, S., Canadell, J. G., Ciais, P.,
1277 Jackson, R. B., Alin, S. R., Alkama, R., Arneeth, A., Arora, V. K., Bates, N. R., Becker, M., Bellouin, N., Bittig,
1278 H. C., Bopp, L., Chevallier, F., Chini, L. P., Cronin, M., Evans, W., Falk, S., Feely, R. A., Gasser, T., Gehlen,
1279 M., Gkritzalis, T., Gloege, L., Grassi, G., Gruber, N., Gürses, Ö., Harris, I., Hefner, M., Houghton, R. A., Hurtt,
1280 G. C., Iida, Y., Ilyina, T., Jain, A. K., Jersild, A., Kadono, K., Kato, E., Kennedy, D., Klein Goldewijk, K.,
1281 Knauer, J., Korsbakken, J. I., Landschützer, P., Lefèvre, N., Lindsay, K., Liu, J., Liu, Z., Marland, G., Mayot, N.,
1282 McGrath, M. J., Metzl, N., Monacchi, N. M., Munro, D. R., Nakaoka, S.-I., Niwa, Y., O'Brien, K., Ono, T.,
1283 Palmer, P. I., Pan, N., Pierrot, D., Pockock, K., Poulter, B., Resplandy, L., Robertson, E., Rödenbeck, C.,
1284 Rodriguez, C., Rosan, T. M., Schwinger, J., Séférian, R., Shutler, J. D., Skjelvan, I., Steinhoff, T., Sun, Q.,
1285 Sutton, A. J., Sweeney, C., Takao, S., Tanhua, T., Tans, P. P., Tian, X., Tian, H., Tilbrook, B., Tsujino, H.,
1286 Tubiello, F., van der Werf, G. R., Walker, A. P., Wanninkhof, R., Whitehead, C., Willstrand Wranne, A.,
1287 Wright, R., Yuan, W., Yue, C., Yue, X., Zaehle, S., Zeng, J., and Zheng, B.: Global Carbon Budget 2022, *Earth*
1288 *Syst. Sci. Data*, 14, 4811–4900, <https://doi.org/10.5194/essd-14-4811-2022>, 2022.
1289
1290 Friedlingstein, P., O'Sullivan, M., Jones, M. W., Andrew, R. M., Bakker, D. C. E., Hauck, J., Landschützer, P.,
1291 Le Quéré, C., Luijkx, I. T., Peters, G. P., Peters, W., Pongratz, J., Schwingshackl, C., Sitch, S., Canadell, J. G.,
1292 Ciais, P., Jackson, R. B., Alin, S. R., Anthoni, P., Barbero, L., Bates, N. R., Becker, M., Bellouin, N., Decharme,
1293 B., Bopp, L., Brasika, I. B. M., Cadule, P., Chamberlain, M. A., Chandra, N., Chau, T.-T.-T., Chevallier, F.,
1294 Chini, L. P., Cronin, M., Dou, X., Enyo, K., Evans, W., Falk, S., Feely, R. A., Feng, L., Ford, D. J., Gasser, T.,
1295 Ghattas, J., Gkritzalis, T., Grassi, G., Gregor, L., Gruber, N., Gürses, Ö., Harris, I., Hefner, M., Heinke, J.,
1296 Houghton, R. A., Hurtt, G. C., Iida, Y., Ilyina, T., Jacobson, A. R., Jain, A., Jarníková, T., Jersild, A., Jiang, F.,
1297 Jin, Z., Joos, F., Kato, E., Keeling, R. F., Kennedy, D., Klein Goldewijk, K., Knauer, J., Korsbakken, J. I.,
1298 Körtzinger, A., Lan, X., Lefèvre, N., Li, H., Liu, J., Liu, Z., Ma, L., Marland, G., Mayot, N., McGuire, P. C.,
1299 McKinley, G. A., Meyer, G., Morgan, E. J., Munro, D. R., Nakaoka, S.-I., Niwa, Y., O'Brien, K. M., Olsen, A.,
1300 Omar, A. M., Ono, T., Paulsen, M., Pierrot, D., Pockock, K., Poulter, B., Powis, C. M., Rehder, G., Resplandy, L.,
1301 Robertson, E., Rödenbeck, C., Rosan, T. M., Schwinger, J., Séférian, R., Smallman, T. L., Smith, S. M.,
1302 Sospedra-Alfonso, R., Sun, Q., Sutton, A. J., Sweeney, C., Takao, S., Tans, P. P., Tian, H., Tilbrook, B., Tsujino,
1303 H., Tubiello, F., van der Werf, G. R., van Ooijen, E., Wanninkhof, R., Watanabe, M., Wimart-Rousseau, C.,
1304 Yang, D., Yang, X., Yuan, W., Yue, X., Zaehle, S., Zeng, J., and Zheng, B.: Global Carbon Budget 2023, *Earth*
1305 *Syst. Sci. Data*, 15, 5301–5369, <https://doi.org/10.5194/essd-15-5301-2023>, 2023.
1306
1307 Fröb, F., Olsen, A., Becker, M., Chafik, L., Johannessen, T., Reverdin, G., and Omar, A.: Wintertime fCO₂
1308 variability in the subpolar North Atlantic since 2004. *Geophysical Research Letters*, 46,
1309 <https://doi.org/10.1029/2018GL080554>, 2019.
1310
1311 Gac, J.-P., Marrec, P., Cariou, T., Grosstefan, E., Macé, E., Rimmelin-Maury, P., Vernet, M., and Bozec, Y.:
1312 Decadal Dynamics of the CO₂ System and Associated Ocean Acidification in Coastal Ecosystems of the North
1313 East Atlantic Ocean. *Front. Mar. Sci.* 8:688008. doi:10.3389/fmars.2021.688008, 2021.
1314
1315 Gallego, M. A., Timmermann, A., Friedrich, T., and Zeebe, R. E.: Drivers of future seasonal cycle changes in
1316 oceanic pCO₂, *Biogeosciences*, 15, 5315–5327, <https://doi.org/10.5194/bg-15-5315-2018>, 2018.
1317
1318 Gattuso, J.-P., Magnan, A., Billé, R., Cheung, W. W. L., Howes, E. L., Joos, F., Allemand, D., Bopp, L., Cooley,
1319 S., Eakin, M., Hoegh-Guldberg, O., Kelly, R. P., Pörtner, H.-O., Rogers, A. D., Baxter, J. M., Laffoley, D.,
1320 Osborn, D., Rankovic, A., Rochette, J., Sumaila, U. R., Treyer, S., and Turley, C.: Contrasting futures for ocean

1321 and society from different anthropogenic CO₂ emissions scenarios. *Science* 349:aac4722.doi:
1322 10.1126/science.aac4722, 2015.

1323

1324 Gattuso, Jean-Pierre; Alliouane, Samir; Mousseau, Laure (2021): Seawater carbonate chemistry in the Bay of
1325 Villefranche, Point B (France), January 2007 - June 2023 [dataset]. PANGAEA,
1326 <https://doi.org/10.1594/PANGAEA.727120>

1327

1328 Gibb, O., Cyr, F., Azetsu-Scott, K., Chassé, J., Childs, D., Gabriel, C.-E., Galbraith, P. S., Maillet, G., Pepin, P.,
1329 Punshon, S., and Starr, M.: Spatiotemporal variability in pH and carbonate parameters on the Canadian Atlantic
1330 continental shelf between 2014 and 2022, *Earth Syst. Sci. Data*, 15, 4127–4162, <https://doi.org/10.5194/essd-15-4127-2023>, 2023.

1331

1332

1333 Goyet, C., Beauverger, C., Brunet, C., and Poisson, A.: Distribution of carbon dioxide partial pressure in surface
1334 waters of the Southwest Indian Ocean, *Tellus B: Chemical and Physical Meteorology*, 43:1, 1-11, DOI:
1335 [10.3402/tellusb.v43i1.15242](https://doi.org/10.3402/tellusb.v43i1.15242), 1991.

1336

1337 Goyet C., Hassoun, A. E. R. Gemayel, E. Touratier, F., Abboud-Abi Saab M. and Guglielmi, V.:
1338 Thermodynamic forecasts of the Mediterranean Sea Acidification. *Mediterranean Marine Science*, 17/2, 508-
1339 518, <http://dx.doi.org/10.12681/mms.1487>, 2016

1340

1341 Goyet C., Benallal, M.A., Bijoux A., Guglielmi, V., Moussa, H., Ribou, A.-C., and Touratier, F.: Ch.39,
1342 Evolution of human Impact on Oceans: Tipping points of socio-ecological Coviability. In: *Coviability of Social
1343 and Ecological Systems: Reconnecting Mankind to the Biosphere in an Era of Global Change*. O.Barrière et al.
1344 (eds.) Springer International Publishing AG, part of Springer Nature 2019. https://doi.org/10.1007/978-3-319-78111-2_12, 2019

1345

1346

1347 Gregor, L. and Gruber, N.: OceanSODA-ETHZ: a global gridded data set of the surface ocean carbonate system
1348 for seasonal to decadal studies of ocean acidification, *Earth Syst. Sci. Data*, 13, 777–808,
1349 <https://doi.org/10.5194/essd-13-777-2021>, 2021.

1350

1351 Gregor, L., Shutler, J., and Gruber, N.: High-resolution variability of the ocean carbon sink. *Global
1352 Biogeochemical Cycles*, 38, e2024GB008127. <https://doi.org/10.1029/2024GB008127>, 2024

1353

1354 Gruber, N., Clement, D. , Carter, B. R., Feely, R. A., van Heuven, S., Hoppema, M., Ishii, M., Key, R. M.,
1355 Kozyr, A., Lauvset, S. K., Lo Monaco, C. , Mathis, J. T., Murata, A., Olsen, A., Perez, F. F., Sabine, C. L.,
1356 Tanhua, T., and Wanninkhof, R.: The oceanic sink for anthropogenic CO₂ from 1994 to 2007, *Science* vol. 363
1357 (issue 6432), pp. 1193-1199. DOI: 10.1126/science.aau5153, 2019.

1358

1359 Guglielmi V., Touratier, F., and Goyet, C.: Design of sampling strategy measurements of CO₂/carbonate
1360 properties. *Journal of Oceanography and Aquaculture*, DOI: 10.23880/ijoac-16000227, 2022

1361

1362 Guglielmi V., Touratier, F., and Goyet, C.: Determination of discrete sampling locations minimizing both the
1363 number of samples and the maximum interpolation error: Application to measurements of carbonate chemistry in
1364 surface ocean, *Journal of Sea Research*, <https://doi.org/10.1016/j.seares.2023.102336>, 2023

1365

1366 Hauck, J., Gregor, L., Nissen, C., Patara, L., Hague, M., Mongwe, P., et al.: The Southern Ocean carbon cycle
1367 1985–2018: Mean, seasonal cycle, trends, and storage. *Global Biogeochemical Cycles*, 37, e2023GB007848.
1368 <https://doi.org/10.1029/2023GB007848>, 2023

1369

1370 Ho, D. T., Bopp, L., Palter, J. B., Long, M. C., Boyd, P.W., Neukermans, G., and Bach, L. T. : Monitoring,
1371 reporting, and verification for ocean alkalinity enhancement. *State of the Planet*, 2-oae2023, 1–12, 2023.

1372

1373 Holliday, N.P., Bersch, M., Berx, B., Chafik, L., Cunningham, S., Florindo-López, C., Hátún, H., Johns, W.,
1374 Josey, S.A., Larsen, K.M.H., Mulet, S., Oltmanns, M., Reverdin, G., Rossby, T., Thierry, V., Valdimarsson, H.,
1375 Yashayev, I. : Ocean circulation causes the largest freshening event for 120 years in eastern subpolar North
1376 Atlantic. *Nat. Commun.*, 11. <https://doi.org/10.1038/s41467-020-14474-y>, 2020
1377
1378 Howes, E., Stemmann, L., Assailly, C., Irisson, J.-O., Dima, M., Bijma, J., Gattuso, J.-P.: Pteropod time series
1379 from the North Western Mediterranean (1967-2003): impacts of pH and climate variability. *Mar Ecol Prog Ser*
1380 531: 193-206, doi: 10.3354/meps11322. 2015.
1381
1382 Huang, B., P. W. Thorne, V. F. Banzon, T. Boyer, G. Chepurin, J. H. Lawrimore, M. J. Menne, T. M. Smith, R.
1383 S. Vose, and H.-M. Zhang: Extended Reconstructed Sea Surface Temperature, version 5 (ERSSTv5): Upgrades,
1384 validations, and intercomparisons. *J. Climate*, 30, 8179-8205, doi:10.1175/JCLI-D-16-0836.1, 2017
1385
1386 IPCC. Changing Ocean, Marine Ecosystems, and Dependent Communities. in *The Ocean and Cryosphere in a*
1387 *Changing Climate 447–588* (Cambridge University Press, 2022). doi:10.1017/9781009157964.007. 2022
1388
1389 Jiang, Z.-P., Tyrrell, T., Hydes, D. J., Dai, M., and Hartman, S. E.: Variability of alkalinity and the alkalinity-
1390 salinity relationship in the tropical and subtropical surface ocean, *Global Biogeochem. Cycles*, 28, 729–742,
1391 doi:10.1002/2013GB004678, 2014.
1392
1393 Jiang, L.-Q., Feely, R. A., Wanninkhof, R., Greeley, D., Barbero, L., Alin, S., Carter, B. R., Pierrot, D.,
1394 Featherstone, C., Hooper, J., Melrose, C., Monacci, N., Sharp, J. D., Shellito, S., Xu, Y.-Y., Kozyr, A., Byrne, R.
1395 H., Cai, W.-J., Cross, J., Johnson, G. C., Hales, B., Langdon, C., Mathis, J., Salisbury, J., and Townsend, D. W.:
1396 Coastal Ocean Data Analysis Product in North America (CODAP-NA) – an internally consistent data product for
1397 discrete inorganic carbon, oxygen, and nutrients on the North American ocean margins. *Earth System Science*
1398 *Data*, 13(6), 2777–2799. <https://doi.org/10.5194/essd-13-2777-2021>, 2021
1399
1400 Jiang, L.-Q., Dunne, J., Carter, B. R., Tjiputra, J. F., Terhaar, J., Sharp, J. D., et al.: Global surface ocean
1401 acidification indicators from 1750 to 2100. *Journal of Advances in Modeling Earth Systems*, 15,
1402 e2022MS003563. <https://doi.org/10.1029/2022MS003563> , 2023
1403
1404 Jiang, L.Q., Fay, A., Müller, J. D. et al: Synthesis products for ocean carbon chemistry. In prep., 2024.
1405
1406 Jing, Y., Li, Y., Xu, Y., and Fan, G.: Influences of the NAO on the North Atlantic CO₂ fluxes in winter and
1407 summer on the interannual scale. *Advances in Atmospheric Sciences*, 36(11), 1288–1298.
1408 <https://doi.org/10.1007/s00376-019-8247-2>, 2019
1409
1410 Kapsenberg, L., Alliouane, S., Gazeau, F., Mousseau, L., and Gattuso, J.-P.: Coastal ocean acidification and
1411 increasing total alkalinity in the northwestern Mediterranean Sea, *Ocean Sci.*, 13, 411-426, doi:10.5194/os-13-
1412 411-2017, 2017.
1413
1414 Khatiwala, S., Tanhua, T., Mikaloff Fletcher, S., Gerber, M., Doney, S. C., Graven, H. D., Gruber, N.,
1415 McKinley, G. A., Murata, A., Ríos, A. F., and Sabine, C. L.: Global ocean storage of anthropogenic carbon,
1416 *Biogeosciences*, 10, 2169-2191, <https://doi.org/10.5194/bg-10-2169-2013>, 2013.
1417
1418 Koffi, U., Lefèvre, N., Kouadio, G., and Boutin, J.: Surface CO₂ parameters and air-sea CO₂ fluxes distribution
1419 in the eastern equatorial Atlantic Ocean. *J. Marine Systems*, doi:10.1016/j.jmarsys/2010.04.010. 2010.
1420
1421 Kwiatkowski, L., Torres, O., Bopp, L., Aumont, O., Chamberlain, M., Christian, J. R., Dunne, J. P., Gehlen, M.,
1422 Ilyina, T., John, J. G., Lenton, A., Li, H., Lovenduski, N. S., Orr, J. C., Palmieri, J., Santana-Falcón, Y.,
1423 Schwinger, J., Séférian, R., Stock, C. A., Tagliabue, A., Takano, Y., Tjiputra, J., Toyama, K., Tsujino, H.,
1424 Watanabe, M., Yamamoto, A., Yool, A., and Ziehn, T.: Twenty-first century ocean warming, acidification,

1425 deoxygenation, and upper-ocean nutrient and primary production decline from CMIP6 model projections,
1426 Biogeosciences, 17, 3439–3470, <https://doi.org/10.5194/bg-17-3439-2020>, 2020.
1427

1428 Lacoue-Labarthe, T., Nunes, P. A. L. D., Ziveri, P., Cinar, M., Gazeau, F., Hall-Spencer, J. M., Hilmi, N.,
1429 Moschella, P., Safa, A., Sauzade, D., and Turley, C.: Impacts of ocean acidification in a warming Mediterranean
1430 Sea: An overview, *Regional Studies in Marine Science*, 5, 1–11, doi:10.1016/j.rsma.2015.12.005, 2016.
1431

1432 Lagoutte, E., A. Tribollet, S. Bureau, et al., Biogeochemical evidence of flow re-entrainment on the main
1433 fringing reef of La Reunion Island, *Marine Chemistry*, <https://doi.org/10.1016/j.marchem.2024.104352>, 2023.
1434

1435 Laika, H. E., Goyet C., Vouve F., Poisson A., and Touratier F. : Interannual properties of the CO₂ system in the
1436 Southern Ocean south of Australia. *Antarctic Science*, 21(6), 663–680.
1437 <https://doi.org/10.1017/S0954102009990319>, 2009
1438

1439 Lan, X., Tans, P. and K.W. Thoning: Trends in globally-averaged CO₂ determined from NOAA Global
1440 Monitoring Laboratory measurements. Version 2024-08 <https://doi.org/10.15138/9NOH-ZH07> (last access: 14
1441 August 2024), 2024.
1442

1443 Landschützer, P., Gruber, N., Bakker, D. C. E., Stemmler, I., and Six, K. D.: Strengthening seasonal marine CO₂
1444 variations due to increasing atmospheric CO₂. *Nature Climate Change*, 8(2), 146–150.
1445 <https://doi.org/10.1038/s41558-017-0057-x>, 2018
1446

1447 Landschützer, P., Ilyina, T., and Lovenduski, N. S. : Detecting regional modes of variability in observation-
1448 based surface ocean pCO₂. *Geophysical Research Letters*, 46. <https://doi.org/10.1029/2018GL081756>, 2019
1449

1450 Lange, N., Fiedler, B., Álvarez, M., Benoit-Cattin, A., Benway, H., Buttigieg, P. L., Coppola, L., Currie, K.,
1451 Flecha, S., Gerlach, D. S., Honda, M., Huertas, I. E., Lauvset, S. K., Muller-Karger, F., Körtzinger, A., O'Brien,
1452 K. M., Ólafsdóttir, S. R., Pacheco, F. C., Rueda-Roa, D., Skjelvan, I., Wakita, M., White, A., and Tanhua, T.:
1453 Synthesis Product for Ocean Time Series (SPOTS) – a ship-based biogeochemical pilot, *Earth Syst. Sci. Data*,
1454 16, 1901–1931, <https://doi.org/10.5194/essd-16-1901-2024>, 2024.
1455

1456 LANSARD Bruno (2014) DICASE cruise, RV Téthys II, <https://doi.org/10.17600/14007100>
1457

1458 Laruelle, G. G., Dürr, H. H., Lauerwald, R., Hartmann, J., Slomp, C. P., Goossens, N., and Regnier, P. A. G.:
1459 Global multi-scale segmentation of continental and coastal waters from the watersheds to the continental
1460 margins, *Hydrol. Earth Syst. Sci.*, 17, 2029–2051, <https://doi.org/10.5194/hess-17-2029-2013>, 2013.
1461

1462 Laruelle, G. G. et al. Continental shelves as a variable but increasing global sink for atmospheric carbon dioxide.
1463 *Nat. Commun.* 9, 454, DOI: 10.1038/s41467-017-02738-z, 2018
1464

1465 Lauvset, S. K., Lange, N., Tanhua, T., Bittig, H. C., Olsen, A., Kozyr, A., Álvarez, M., Azetsu-Scott, K., Brown,
1466 P. J., Carter, B. R., Cotrim da Cunha, L., Hoppema, M., Humphreys, M. P., Ishii, M., Jeansson, E., Murata, A.,
1467 Müller, J. D., Pérez, F. F., Schirnick, C., Steinfeldt, R., Suzuki, T., Ulfsbo, A., Velo, A., Woosley, R. J., and
1468 Key, R. M.: The annual update GLODAPv2.2023: the global interior ocean biogeochemical data product, *Earth*
1469 *Syst. Sci. Data*, 16, 2047–2072, <https://doi.org/10.5194/essd-16-2047-2024>, 2024.
1470

1471 Lefèvre, D.: MOOSE (ANTARES), <https://doi.org/10.18142/233>, 2010.
1472

1473 Lefèvre N.: Carbon parameters along a zonal transect. SEANOE. <https://doi.org/10.17882/58575>, 2010.
1474

1475 Lefèvre Nathalie (2017). Carbon parameters in the gulf of Maranhao. SEANOE. <https://doi.org/10.17882/62417>
1476

1477 Lefèvre Nathalie (2018). Carbon parameters in the Western tropical Atlantic. SEANOE.
1478 <https://doi.org/10.17882/58406>
1479

1480 Lefèvre Nathalie (2019). Carbon parameters in the Eastern Tropical Atlantic in 2019. SEANOE.
1481 <https://doi.org/10.17882/83682>
1482

1483 Lefèvre Nathalie (2020). Inorganic carbon and alkalinity in the Eastern tropical Atlantic measured during the
1484 PIRATA FR-30 cruise in February-March 2020. SEANOE. <https://doi.org/10.17882/90742>
1485

1486 Lefèvre Nathalie (2022). Inorganic carbon and alkalinity in the Eastern tropical Atlantic in 2022. SEANOE.
1487 <https://doi.org/10.17882/92386>
1488

1489 Lefèvre, N., Urbano, D.F., Gallois, F., and Diverrès, D.: Impact of physical processes on the seasonal
1490 distribution of CO₂ in the western tropical Atlantic. *Journal of Geophysical Research* 119,
1491 doi: 10.1002/2013JC009248. doi: DOI: 10.1002/2013JC009248, 2014
1492

1493 Lefèvre, N., Veleda, D., Araujo, M., Caniaux, G.: Variability and trends of carbon parameters at a time series in
1494 the eastern tropical Atlantic. *Tellus B*, Co-Action Publishing, 68, pp.30305. 10.3402/tellusb.v68.30305. 2016.
1495

1496 Lefèvre N., da Silva Dias F. J., de Torres A. R., Noriega C., Araujo M., de Castro A. C. L., Rocha C., Jiang S.,
1497 Ibánhez J. S. P.: A source of CO₂ to the atmosphere throughout the year in the Maranhense continental shelf
1498 (2°30'S, Brazil). *Continental Shelf Research*, 141, 38-50. <https://doi.org/10.1016/j.csr.2017.05.004>, 2017a
1499

1500 Lefèvre N., Flores Montes M., Gaspar F. L., Rocha C., Jiang S., De Araújo M. C., Ibánhez J. S. P.: Net
1501 Heterotrophy in the Amazon Continental Shelf Changes Rapidly to a Sink of CO₂ in the Outer Amazon Plume.
1502 *Frontiers in Marine Science*, 4, -. <https://doi.org/10.3389/fmars.2017.00278>, 2017b
1503

1504 Lefèvre, N., Mejia, C., Khvorostyanov, D., Beaumont, L., and Koffi, U.: Ocean Circulation Drives the
1505 Variability of the Carbon System in the Eastern Tropical Atlantic. *Oceans*, 2021, 2, 126–148.
1506 <https://doi.org/10.3390/oceans2010008>, 2021.
1507

1508 Lefèvre, N., Veleda, D., Hartman, S.E.: Outgassing of CO₂ dominates in the coastal upwelling off the northwest
1509 African coast, *Deep-Sea Research Part I*, doi: <https://doi.org/10.1016/j.dsr.2023.104130>, 2023
1510

1511 Lefèvre, N., Veleda, D. and Beaumont; L.: Trends and drivers of CO₂ parameters, from 2006 to 2021, at a time-
1512 series station in the Eastern Tropical Atlantic (6°S, 10°W). *Front. Mar. Sci.* 11:1299071. doi:
1513 10.3389/fmars.2024.1299071, 2024
1514

1515 Leseurre, C.: Mécanismes de contrôle de l'absorption de CO₂ anthropique et de l'acidification des eaux dans les
1516 océans Atlantique Nord et Austral. PhD Thesis, Sorbonne Univ., 270 pp. <https://theses.hal.science/tel-04028410>,
1517 2022
1518

1519 Leseurre, C., Lo Monaco, C., Reverdin, G., Metzl, N., Fin, J., Olafsdottir, S., and Racapé, V.: Ocean carbonate
1520 system variability in the North Atlantic Subpolar surface water (1993–2017), *Biogeosciences*, 17, 2553–2577,
1521 <https://doi.org/10.5194/bg-17-2553-2020>, 2020
1522

1523 Leseurre, C., Lo Monaco, C., Reverdin, G., Metzl, N., Fin, J., Mignon, C., and Benito, L.: Summer trends and
1524 drivers of sea surface fCO₂ and pH changes observed in the southern Indian Ocean over the last two decades
1525 (1998–2019), *Biogeosciences*, 19, 2599–2625, <https://doi.org/10.5194/bg-19-2599-2022>, 2022.
1526

1527 Li, X., et al.: The source and accumulation of anthropogenic carbon in the U.S. East Coast, *Sci. Adv.* 10,
1528 ead13169, DOI: 10.1126/sciadv.ad13169, 2024
1529

1530 LO MONACO Claire, METZL Nicolas (2019) VT 163 / OISO-29 cruise, RV Marion Dufresne,
1531 <https://doi.org/10.17600/18000972>
1532

1533 LO MONACO Claire (2020) OISO-30 cruise, RV Marion Dufresne, <https://doi.org/10.17600/18000679>
1534

1535 LO MONACO Claire, JEANDEL Catherine, PLANQUETTE H el ene (2021) OISO-31 cruise, RV Marion
1536 Dufresne, <https://doi.org/10.17600/18001254>
1537

1538 Lo Monaco, Claire; Metzl, Nicolas; Fin, Jonathan (2022). Sea surface measurements of dissolved inorganic
1539 carbon (DIC), total alkalinity (TALK), temperature and salinity during the R/V Marion-Dufresne Ocean Indien
1540 Service d'Observations - 29 (OISO-29) cruise (EXPOCODE 35MV20190106) in the Indian Ocean from 2019-
1541 01-06 to 2019-02-09 (NCEI Accession 0252612). NOAA National Centers for Environmental Information.
1542 Dataset. <https://doi.org/10.25921/8ajx-za24>. Accessed 14-Aug-2024.
1543

1544 Lo Monaco, Claire; Metzl, Nicolas (2023). Sea surface measurements of dissolved inorganic carbon (DIC), total
1545 alkalinity (TALK), temperature and salinity during the R/V Marion-Dufresne Ocean Indien Service
1546 d'Observations - 30 (OISO-30) cruise (EXPOCODE 35MV20200106) in the Indian Ocean from 2020-01-06 to
1547 2020-02-01 (NCEI Accession 0280937). NOAA National Centers for Environmental Information. Dataset.
1548 <https://doi.org/10.25921/n2g0-pp38>. Accessed 14-Aug-2024
1549

1550 Lo Monaco, Claire; Metzl, Nicolas; Fin, Jonathan (2023). Sea surface measurements of dissolved inorganic
1551 carbon (DIC), total alkalinity (TALK), temperature and salinity during the R/V Marion-Dufresne Ocean
1552 Indien Service d'Observations - 31 (OISO-31) cruise (EXPOCODE 35MV20210113) in the Indian Ocean
1553 from 2021-01-14 to 2021-03-04 (NCEI Accession 0280946). NOAA National Centers for Environmental
1554 Information. Dataset. <https://doi.org/10.25921/7sb2-k852>. Accessed 14-Aug-2024
1555

1556 Mathis, M., Lacroix, F., Hagemann, S. et al.: Enhanced CO2 uptake of the coastal ocean is dominated by
1557 biological carbon fixation. *Nat. Clim. Chang.* <https://doi.org/10.1038/s41558-024-01956-w>, 2024
1558

1559 Maugendre, L., J.-P. Gattuso, J. Louis, A. de Kluijver, S. Marro, K. Soetaert, F. Gazeau: Effect of ocean
1560 warming and acidification on a plankton community in the NW Mediterranean Sea, *ICES Journal of Marine
1561 Science*, Volume 72, Issue 6, July/August 2015, Pages 1744–1755, <https://doi.org/10.1093/icesjms/fsu161>, 2015
1562

1563 Mercier, H., Lherminier, P., Sarafanov, A., Gaillard, F., Daniault, N., Desbry eres, D., Falina, A., Ferron, B.,
1564 Huck, T., and Thierry, V.: Variability of the meridional overturning circulation at the Greenland-Portugal Ovide
1565 section from 1993 to 2010. *Progress in Oceanography*, 132, 250-261, [doi:10.1016/j.pocean.2013.11.001](https://doi.org/10.1016/j.pocean.2013.11.001). 2015
1566

1567 Mercier, H., Desbry eres, D., Lherminier, P., Velo, A., Carracedo, L., Fontela, M., and P erez, F. F.: New
1568 insights into the eastern subpolar North Atlantic meridional overturning circulation from OVIDE, *Ocean Sci.*,
1569 20, 779–797, <https://doi.org/10.5194/os-20-779-2024>, 2024.
1570

1571 Metzl, N., Brunet, C., Jabaud-Jan, A., Poisson, A., and Schauer, B.: Summer and winter air-sea CO2 fluxes in
1572 the Southern Ocean *Deep Sea Res I*, 53, 1548-1563, [doi:10.1016/j.dsr.2006.07.006](https://doi.org/10.1016/j.dsr.2006.07.006). 2006.
1573

1574 Metzl, N., Corbi ere, A., Reverdin, G., Lenton, A., Takahashi, T., Olsen, A., Johannessen, T., Pierrot, D.,
1575 Wanninkhof, R.,  lafsd ottir, S. R., Olafsson, J., and Ramonet, M.: Recent acceleration of the sea surface fCO2
1576 growth rate in the North Atlantic subpolar gyre (1993-2008) revealed by winter observations, *Global
1577 Biogeochem. Cycles*, 24, GB4004, [doi:10.1029/2009GB003658](https://doi.org/10.1029/2009GB003658), 2010.
1578

1579 Metzl, N., and Lo Monaco, C.: OISO - OC EAN INDIEN SERVICE D'OBSERVATION,
1580 <https://doi.org/10.18142/228>, 1998.
1581

1582 Metz, N., Lo Monaco, C., Leseurre, C., Ridame, C., Fin, J., Mignon, C., Gehlen, M., and Chau, T. T. T.: The
1583 impact of the South-East Madagascar Bloom on the oceanic CO₂ sink, *Biogeosciences*, 19, 1451–1468,
1584 <https://doi.org/10.5194/bg-19-1451-2022>, 2022
1585

1586 Metz, N., Fin, J., Lo Monaco, C., Mignon, C., Alliouane, S., Antoine, D., Bourdin, G., Boutin, J., Bozec, Y.,
1587 Guillaume, G., Boutin, J., Bozec, Y., Conan, P., Coppola, L., Diaz, F., Douville, E., Durrieu de Madron, X.,
1588 Gattuso, J.-P., Gazeau, F., Golbol, M., Lansard, B., Lefèvre, D., Lefèvre, N., Lombard, F., Louanchi, F.,
1589 Merlivat, L., Olivier, L., Petrenko, A., Petton, S., Pujo-Pay, M., Rabouille, C., Reverdin, G.,
1590 Ridame, C., Tribollet, A., Vellucci, V., Wagener, T., and Wimart-Rousseau, C.: A synthesis of ocean total
1591 alkalinity and dissolved inorganic carbon observations in the global ocean (1993–2022). *SEANOE*.
1592 <https://doi.org/10.17882/95414>, 2023
1593
1594

1595 Metz, N., Fin, J., Lo Monaco, C., Mignon, C., Alliouane, S., Antoine, D., Bourdin, G., Boutin, J., Bozec, Y.,
1596 Conan, P., Coppola, L., Diaz, F., Douville, E., Durrieu de Madron, X., Gattuso, J.-P., Gazeau, F., Golbol, M.,
1597 Lansard, B., Lefèvre, D., Lefèvre, N., Lombard, F., Louanchi, F., Merlivat, L., Olivier, L., Petrenko, A.,
1598 Petton, S., Pujo-Pay, M., Rabouille, C., Reverdin, G., Ridame, C., Tribollet, A., Vellucci, V., Wagener, T.,
1599 and Wimart-Rousseau, C.: A synthesis of ocean total alkalinity and dissolved inorganic carbon measurements
1600 from 1993 to 2022: the SNAPO-CO₂-v1 dataset, *Earth Syst. Sci. Data*, 16, 89–120, <https://doi.org/10.5194/essd-16-89-2024>,
1601 2024a
1602

1603 Metz, N., Lo Monaco, C., Leseurre, C., Ridame, C., Reverdin, G., Chau, T. T. T., Chevallier, F., and Gehlen,
1604 M.: Anthropogenic CO₂, air–sea CO₂ fluxes, and acidification in the Southern Ocean: results from a time-series
1605 analysis at station OISO-KERFIX (51° S–68° E), *Ocean Sci.*, 20, 725–758, [https://doi.org/10.5194/os-20-725-](https://doi.org/10.5194/os-20-725-2024)
1606 2024, 2024b.
1607

1608 Metz, N., Lo Monaco, C., Barut, G., and TERNON, J.-F.: Contrasting trends of the ocean CO₂ sink and pH in the
1609 Agulhas current system and the Mozambique Basin, South-Western Indian Ocean (1963–2023). *Deep Sea Res.*,
1610 special issue IIOE-2, in rev., 2024c
1611

1612 Metz, N., Fin, J., Lo Monaco, C., Mignon, C., Alliouane, S., Bombled, B., Boutin, J., Bozec, Y., Comeau,
1613 S., Conan, P., Coppola, L., Cuet, P., Ferreira, E., Gattuso, J.-P., Gazeau, F., Goyet, C., Grossteffan, E.,
1614 Lansard, B., Lefèvre, D., Lefèvre, N., Lombard, F., Louanchi, F., Merlivat, L., Olivier, L., Petrenko, A.,
1615 Petton, S., Pujo-Pay, M., Rabouille, C., Reverdin, G., Ridame, C., Rimmel, M., TERNON, J.-F., Touratier,
1616 F., Tribollet, A., Wagener, T., and Wimart-Rousseau, C.: An updated synthesis of ocean total alkalinity and
1617 dissolved inorganic carbon measurements from 1993 to 2023: the SNAPO-CO₂-v2 dataset. *SEANOE*.
1618 <https://doi.org/10.17882/102337>, 2024d
1619

1620 MICHEL, E., and VIVIER, F.: STEP 2016 cruise, RV L'Atalante, <https://doi.org/10.17600/16000900>,
1621 2016
1622

1623 Mu, L., Gomes, H. do R., Burns, S. M., Goes, J. I., Coles, V. J., Rezende, C. E., et al.: Temporal Variability of
1624 Air-Sea CO₂ flux in the Western Tropical North Atlantic Influenced by the Amazon River Plume. *Global
1625 Biogeochemical Cycles*, 35(6). <https://doi.org/10.1029/2020GB006798>, 2021
1626

1627 Munro, D. R., Lovenduski, N. S., Takahashi, T., Stephens, B. B., Newberger, T., and Sweeney, C.: Recent
1628 evidence for a strengthening CO₂ sink in the Southern Ocean from carbonate system measurements in the Drake
1629 Passage (2002–2015), *Geophys. Res. Lett.*, 42, 7623–7630, <https://doi.org/10.1002/2015GL065194>, 2015.
1630

1631 Müller, J. D., Gruber, N., Carter, B., Feely, R., Ishii, M., Lange, N., et al.: Decadal trends in the oceanic storage
1632 of anthropogenic carbon from 1994 to 2014. *AGU Advances*, 4, e2023AV000875.
1633 <https://doi.org/10.1029/2023AV000875>, 2023
1634

1635
1636 Newton, J.A., Feely, R. A., Jewett, E. B., Williamson, P. and Mathis, J.: Global Ocean Acidification Observing
1637 Network: Requirements and Governance Plan. Second Edition, GOA-ON,
1638 <https://www.iaea.org/sites/default/files/18/06/goa-on-second-edition-2015.pdf>, 2015.
1639
1640 Olafsson, J., Olafsdottir, S. R., Benoit-Cattin, A., and Takahashi, T.: The Irminger Sea and the Iceland Sea time
1641 series measurements of sea water carbon and nutrient chemistry 1983–2008, *Earth Syst. Sci. Data*, 2, 99–104,
1642 <https://doi.org/10.5194/essd-2-99-2010>, 2010.
1643
1644 Olivier, L., Boutin, J., Reverdin, G., Lefèvre, N., Landschützer, P., Speich, S., Karstensen, J., Labaste, M.,
1645 Noisel, C., Ritschel, M., Steinhoff, T., and Wanninkhof, R.: Wintertime process study of the North Brazil
1646 Current rings reveals the region as a larger sink for CO₂ than expected, *Biogeosciences*, 19, 2969–2988,
1647 <https://doi.org/10.5194/bg-19-2969-2022>, 2022.
1648
1649 Olsen, A., Key, R. M., van Heuven, S., Lauvset, S. K., Velo, A., Lin, X., Schirnick, C., Kozyr, A., Tanhua, T.,
1650 Hoppema, M., Jutterström, S., Steinfeldt, R., Jeansson, E., Ishii, M., Pérez, F. F., and Suzuki, T.: The Global
1651 Ocean Data Analysis Project version 2 (GLODAPv2) – an internally consistent data product for the world ocean,
1652 *Earth Syst. Sci. Data*, 8, 297–323, <https://doi.org/10.5194/essd-8-297-2016>, 2016.
1653
1654 Oudot, C., Ternon, J. F., and Lecomte, J.: Measurements of atmospheric and oceanic CO₂ in the tropical Atlantic:
1655 10 years after the 1982–1984 FOCAL cruises. *Tellus B: Chemical and Physical Meteorology*, 47(1–2), 70–85.
1656 <https://doi.org/10.3402/tellusb.v47i1-2.16032>, 1995
1657
1658 Padin, X. A., Velo, A., and Pérez, F. F.: ARIOS: a database for ocean acidification assessment in the Iberian
1659 upwelling system (1976–2018), *Earth Syst. Sci. Data*, 12, 2647–2663, [https://doi.org/10.5194/essd-12-2647-](https://doi.org/10.5194/essd-12-2647-2020)
1660 2020, 2020.
1661
1662 Palacio-Castro, A. M., Enochs, I. C., Besemer, N., Boyd, A., Jankulak, M., Kolodziej, G., et al.: Coral reef
1663 carbonate chemistry reveals interannual, seasonal, and spatial impacts on ocean acidification off Florida. *Global*
1664 *Biogeochemical Cycles*, 37, e2023GB007789. <https://doi.org/10.1029/2023GB007789>, 2023
1665
1666 Pardo, P. C., Tilbrook, B., Langlais, C., Trull, T. W., and Rintoul, S. R.: Carbon uptake and biogeochemical
1667 change in the Southern Ocean, south of Tasmania. *Biogeosciences*, 14(22), 5217–5237.
1668 <https://doi.org/10.5194/bg-14-5217-2017>, 2017.
1669
1670 Pérez, F. F., Becker, M., Goris, N., Gehlen, M., López-Mozos, M., Tjiputra, J., et al.: An assessment of CO₂
1671 storage and sea-air fluxes for the Atlantic Ocean and Mediterranean Sea between 1985 and 2018. *Global*
1672 *Biogeochemical Cycles*, 38, e2023GB007862. <https://doi.org/10.1029/2023GB007862>, 2024
1673
1674 Petton, S., Pernet, F., Le Roy, V., Huber, M., Martin, S., Macé, É., Bozec, Y., Loisel, S., Rimmelin Maury, P.,
1675 Grossteffan, É., Repecaud, M., Quemener, L., Retho, M., Manac'h, S., Papin, M., Pineau, P., Lacoue-Labarthe,
1676 T., Deborde, J., Costes, L., Polsenaere, P., Rigouin, L., Benhamou, J., Gouriou, L., Lequeux, J., Labourdette, N.,
1677 Savoye, N., Messiaen, G., Foucault, E., Ouisse, V., Richard, M., Lagarde, F., Voron, F., Kempf, V., Mas, S.,
1678 Giannecchini, L., Vidussi, F., Mostajir, B., Leredde, Y., Alliouane, S., Gattuso, J.-P., and Gazeau, F.: French
1679 coastal network for carbonate system monitoring: the CocoriCO₂ dataset, *Earth Syst. Sci. Data*, 16, 1667–1688,
1680 <https://doi.org/10.5194/essd-16-1667-2024>, 2024.
1681
1682 Petton Sébastien, Pernet Fabrice, Le Roy Valerian, Huber Matthias, Martin Sophie, Mace Eric, Bozec Yann,
1683 Loisel Stéphane, Rimmelin-Maury Peggy, Grossteffan Emilie, Repecaud Michel, Quémener Loïc, Retho
1684 Michael, Manach Soazig, Papin Mathias, Pineau Philippe, Lacoue-Labarthe Thomas, Deborde Jonathan, Costes
1685 Louis, Polsenaere Pierre, Rigouin Loic, Benhamou Jeremy, Gouriou Laure, Lequeux Joséphine, Labourdette
1686 Nathalie, Savoye Nicolas, Messiaen Gregory, Foucault Elodie, Lagarde Franck, Richard Marion, Ouisse
1687 Vincent, Voron Florian, Mas Sébastien, Giannecchini Léa, Vidussi Francesca, Mostajir Behzad, Leredde Yann,

1688 Kempf Valentin, Alliouane Samir, Gattuso Jean-Pierre, Gazeau Frédéric: French coastal carbonate dataset from
1689 the CocoriCO2 project. SEANOE. <https://doi.org/10.17882/96982>, 2023
1690
1691 Poisson, A., Culkin, F., and Ridout, P.: Intercomparison of CO2 measurements. Deep Sea Research Part A.
1692 Oceanographic Research Papers, 37, 10, 1647-1650, [https://doi.org/10.1016/0198-0149\(90\)90067-6](https://doi.org/10.1016/0198-0149(90)90067-6), 1990.
1693
1694 Pozzato, L., Rassmann, J., Lansard, B., Dumoulin, J.-P., Van Breugel, P., and Rabouille, C.: Origin of
1695 remineralized organic matter in sediments from the Rhone River prodelta (NW Mediterranean) traced by Delta
1696 C-14 and delta C-13 signatures of pore water DIC. Progress In Oceanography, 163, 112-122.
1697 <https://doi.org/10.1016/j.pocean.2017.05.008>, 2018
1698
1699 RABOUILLE Christophe (2010) MESURHOBENT 1 cruise, RV Téthys II, <https://doi.org/10.17600/10450020>
1700
1701 RABOUILLE Christophe (2013) CARBODELTA cruise, RV Téthys II, <https://doi.org/10.17600/13450060>
1702
1703 RABOUILLE Christophe (2018) MISSRHODIA2 cruise, RV Téthys II, <https://doi.org/10.17600/18000473>
1704
1705 RABOUILLE Christophe, BOURRIN François, BASSETTI Maria-Angela (2022) DELTARHONE-1 cruise, RV
1706 Téthys II, <https://doi.org/10.17600/18002027>
1707
1708 Regnier, P., Friedlingstein, P., Ciais, P., Mackenzie, F. T., Gruber, N., et al: Anthropogenic perturbation of the
1709 carbon fluxes from land to ocean. Nat. Geosci. 6:597–607, 2013.
1710
1711 Resplandy, L., Hogikyan, A., Müller, J. D., Najjar, R. G., Bange, H. W., Bianchi, D., et al.: A synthesis of global
1712 coastal ocean greenhouse gas fluxes. Global Biogeochemical Cycles, 38, e2023GB007803.
1713 <https://doi.org/10.1029/2023GB007803>, 2024
1714
1715 Revelle, R., and Suess, H. E.: Carbon dioxide exchange between atmosphere and ocean and the question of an
1716 increase of atmospheric CO2 during the past decades. Tellus 9, 18–27. doi:10.1111/j.2153-
1717 3490.1957.tb01849.x., 1957.
1718
1719 Reverdin, G., Metzl, N., Olafsdottir, S., Racapé, V., Takahashi, T., Benetti, M., Valdimarsson, H., Benoit-Cattin,
1720 A., Danielsen, M., Fin, J., Naamar, A., Pierrot, D., Sullivan, K., Bringas, F., and Goni, G.: SURATLANT: a
1721 1993–2017 surface sampling in the central part of the North Atlantic subpolar gyre, Earth Syst. Sci. Data, 10,
1722 1901-1924, <https://doi.org/10.5194/essd-10-1901-2018>, 2018.
1723
1724 Reverdin, G., Metzl, N., Olafsdottir, S., Racapé, V., Takahashi, T., Benetti, M., Valdimarsson, H., Quay, P. D.,
1725 Benoit-Cattin, A., Danielsen, M., Fin, J., Naamar, A., Pierrot, D., Sullivan, K., Bringas, F., Goni, G., Becker M.,
1726 Leseurre C., and Olsen A.: SURATLANT: a surface dataset in the central part of the North Atlantic subpolar
1727 gyre. SEANOE. <https://doi.org/10.17882/54517>, 2023.
1728
1729 Rodgers, K. B., Schwinger, J., Fassbender, A. J., Landschützer, P., Yamaguchi, R., Frenzel, H., et al.: Seasonal
1730 variability of the surface ocean carbon cycle: A synthesis. Global Biogeochemical Cycles, 37, e2023GB007798.
1731 <https://doi.org/10.1029/2023GB007798>, 2023
1732
1733 Roobaert, A., Resplandy, L., Laruelle, G. G., Liao, E., and Regnier, P. : Unraveling the physical and biological
1734 controls of the global coastal CO2 sink. Global Biogeochemical Cycles, 38, e2023GB007799.
1735 <https://doi.org/10.1029/2023GB007799>, 2024a
1736
1737 Roobaert, A., Regnier, P., Landschützer, P., and Laruelle, G. G.: A novel sea surface pCO2-product for the
1738 global coastal ocean resolving trends over 1982–2020, Earth Syst. Sci. Data, 16, 421–441,
1739 <https://doi.org/10.5194/essd-16-421-2024>, 2024b.
1740

1741 Sarma, V. V. S. S., Krishna, M. S., Paul, Y. S., and Murty, V. S. N.: Observed changes in ocean acidity and
1742 carbon dioxide exchange in the coastal bay of Bengal—A link to air pollution. *Tellus B: Chemical and Physical*
1743 *Meteorology*, 67(1), 24638. <https://doi.org/10.3402/tellusb.v67.24638>, 2015
1744
1745 Sarma, V. V. S. S., Sridevi, B., Metz, N., Patra, P. K., Lachkar, Z., Chakraborty, K., et al. : Air-sea fluxes of
1746 CO₂ in the Indian Ocean between 1985 and 2018: A synthesis based on observation-based surface CO₂, hindcast
1747 and atmospheric inversion models. *Global Biogeochemical Cycles*, 37, e2023GB007694.
1748 <https://doi.org/10.1029/2023GB007694>, 2023
1749
1750 Sarmiento, J.L., Johnson, K.S., Arteaga, L.A., Bushinsky, S.M., Cullen, H.M., Gray, A.R., Hotinski, R.M.,
1751 Maurer, T.L., Mazloff, M.R., Riser, S.C., Russell, J.L., Schofield, O.M., Talley, L.D., The Southern Ocean
1752 Carbon and Climate Observations and Modeling (SOCCOM) project: A review, *Progress in Oceanography*, doi:
1753 <https://doi.org/10.1016/j.pocean.2023.103130>, 2023
1754
1755 Schlitzer, R.: Ocean Data View, Ocean Data View, <http://odv.awi.de> (last access: 13 March 2019), 2018.
1756
1757 Schneider, A., Wallace, D. W. R., and Körtzinger, A.: Alkalinity of the Mediterranean Sea, *Geophys. Res. Lett.*,
1758 34, L15608, doi:10.1029/2006GL028842, 2007.
1759
1760 Schuster, U., McKinley, G. A., Bates, N., Chevallier, F., Doney, S. C., Fay, A. R., González-Dávila, M., Gruber,
1761 N., Jones, S., Krijnen, J., Landschützer, P., Lefèvre, N., Manizza, M., Mathis, J., Metz, N., Olsen, A., Rios, A.
1762 F., Rödenbeck, C., Santana-Casiano, J. M., Takahashi, T., Wanninkhof, R., and Watson, A. J.: An assessment of
1763 the Atlantic and Arctic sea–air CO₂ fluxes, 1990–2009, *Biogeosciences*, 10, 607–627,
1764 <https://doi.org/10.5194/bg-10-607-2013>, 2013.
1765
1766 Shadwick, E., Rintoul, S., Tilbrook, B., Williams, G., Young, N., Fraser, A. D., et al.: Glacier tongue calving
1767 reduced dense water formation and enhanced carbon uptake. *Geophysical Research Letters*, 40(5), 904–909.
1768 <https://doi.org/10.1002/grl.50178>, 2013
1769
1770 Shadwick, E. H., B. Tilbrook, and G. D. Williams: Carbonate chemistry in the Mertz Polynya (East Antarctica):
1771 Biological and physical modification of dense water outflows and the export of anthropogenic CO₂, *J. Geophys.*
1772 *Res. Oceans*, 119, 1–14, doi:10.1002/2013JC009286, 2014
1773
1774 Shadwick, E. H., T. W. Trull, B. Tilbrook, A. J. Sutton, E. Schulz, and C. L. Sabine: Seasonality of biological
1775 and physical controls on surface ocean CO₂ from hourly observations at the Southern Ocean Time Series site
1776 south of Australia, *Global Biogeochem. Cycles*, 29, 223–238, doi:10.1002/2014GB004906, 2015
1777
1778 Shadwick, E. H., Wynn-Edwards, C. A., Matear, R. J., Jansen, P., Schulz, E. and Sutton, A. J.: Observed
1779 amplification of the seasonal CO₂ cycle at the Southern Ocean Time Series. *Front. Mar. Sci.* 10:1281854. doi:
1780 10.3389/fmars.2023.1281854, 2023
1781
1782 Siddiqui, A. H., Haine, T. W. N., Nguyen, A. T., and Buckley, M. W.: Controls on upper ocean salinity
1783 variability in the eastern subpolar North Atlantic during 1992–2017. *Journal of Geophysical*
1784 *Research: Oceans*, 129, e2024JC020887. <https://doi.org/10.1029/2024JC020887>, 2024
1785
1786 Sridevi, B., and Sarma, V. V. S. S.: Role of river discharge and warming on ocean acidification and pco₂ levels
1787 in the Bay of Bengal. *Tellus B: Chemical and Physical Meteorology*, 73 (1), 1–20., DOI:
1788 10.1080/16000889.2021.1971924, 2021
1789
1790 Sutton, A.J., Battisti, R., Carter, B., Evans, W., Newton, J., Alin, S., Bates, N.R., Cai, W.-J., Currie, K., Feely,
1791 R.A., Sabine, C., Tanhua, T., Tilbrook, B., and Wanninkhof, R.: Advancing best practices for assessing trends
1792 of ocean acidification time series. *Frontiers in Marine Science*, 9: 1045667. doi: 10.3389/fmars.2022.1045667,
1793 2022

1794

1795 Takahashi, T., Sutherland, S. C., Wanninkhof, R., Sweeney, C., Feely, R. A., Chipman, D. W., Hales, B.,
1796 Friederich, G., Chavez, F., Sabine, C., Watson, A. J., Bakker, D. C., Schuster, U., Metzl, N., Yoshikawa-Inoue,
1797 H., Ishii, M., Midorikawa, T., Nojiri, Y., Körtzinger, A., Steinhoff, T., Hoppema, M., Olafsson, J., Arnarson, T.
1798 S., Tilbrook, B., Johannessen, T., Olsen, A., Bellerby, R., Wong, C., Delille, B., Bates, N., and de Baar, H. J.:
1799 Climatological mean and decadal change in surface ocean pCO₂, and net sea air CO₂ flux over the global
1800 oceans. *Deep-Sea Res. II*, 56 (8-10), 554–577, <http://dx.doi.org/10.1016/j.dsr2.2008.12.009>. 2009.

1801

1802 Takahashi, T., Sutherland, S. C., Chipman, D. W., Goddard, J. G., Ho, C., Newberger, T., Sweeney, C. and
1803 Munro, D. R.: Climatological distributions of pH, pCO₂, total CO₂, alkalinity, and CaCO₃ saturation in the
1804 global surface ocean, and temporal changes at selected locations. *Marine Chemistry*, 164, 95–125,
1805 doi:10.1016/j.marchem.2014.06.004. 2014.

1806

1807 TERNON, J.-F., OUDOT, C., DESSIER, A., DIVERRES, D.: A seasonal tropical sink for atmospheric CO₂ in the Atlantic
1808 ocean: the role of the Amazon River discharge, *Marine Chemistry*, Volume 68, Issue 3, Pages 183-201,
1809 [https://doi.org/10.1016/S0304-4203\(99\)00077-8](https://doi.org/10.1016/S0304-4203(99)00077-8), 2000

1810

1811 TESTOR Pierre, COPPOLA Laurent, BOSSE Anthony (2021) MOOSE-GE 2021 cruise, RV Thalassa,
1812 <https://doi.org/10.17600/18001333>

1813

1814 TESTOR Pierre, COPPOLA Laurent, BOSSE Anthony (2022) MOOSE-GE 2022 cruise, RV Pourquoi pas ?,
1815 <https://doi.org/10.17600/18001854>

1816

1817 TESTOR Pierre, DURRIEU de MADRON Xavier (2023) MOOSE-GE 2023 cruise, RV Thalassa,
1818 <https://doi.org/10.17600/18002686>

1819

1820 Thomas, H., Prowe, A. E. F., Lima, I. D., Doney, S. C., Wanninkhof, R., Greatbatch, R. J., Schuster, U. and
1821 Corbière, A.: Changes in the North Atlantic Oscillation influence CO₂ uptake in the North Atlantic over the past
1822 2 decades, *Global Biogeochemical Cycles*, 22(4), doi:10.1029/2007GB003167, 2008

1823

1824 Tilbrook, B., Jewett, E. B., DeGrandpre, M. D., Hernandez-Ayon, J. M., Feely, R. A., Gledhill, D. K., Hansson,
1825 L., Isensee, K., Kurz, M. L., Newton, J. A., Siedlecki, S. A., Chai, F., Dupont, S., Graco, M., Calvo, E., Greeley,
1826 D., Kapsenberg, L., Lebec, M., Pelejero, C., Schoo, K. L., and Telszewski, M.: An Enhanced Ocean
1827 Acidification Observing Network: From People to Technology to Data Synthesis and Information Exchange.
1828 *Frontiers in Marine Science*, 6, 337, DOI:10.3389/fmars.2019.00337, 2019.

1829

1830 TOURATIER Franck, POISSON Alain (1990) MINERVE, <https://doi.org/10.18142/128>

1831

1832 Touratier, F., and Goyet, C.: Decadal evolution of anthropogenic CO₂ in the north western Mediterranean Sea
1833 from the mid-1990's to the mid-2000's. *Deep Sea Research Part I*.doi:10.1016/j.dsr.2009.05.015, 2009.

1834

1835 Ulses, C., Estournel, C., Fourier, M., Coppola, L., Kessouri, F., Lefèvre, D., and Marsaleix, P.: Oxygen budget
1836 of the north-western Mediterranean deep- convection region, *Biogeosciences*, 18, 937–960,
1837 <https://doi.org/10.5194/bg-18-937-2021>, 2021.

1838

1839 Ulses, C., Estournel, C., Marsaleix, P., Soetaert, K., Fourier, M., Coppola, L., Lefèvre, D., Touratier, F., Goyet,
1840 C., Guglielmi, V., Kessouri, F., Testor, P., and Durrieu de Madron, X.: Seasonal dynamics and annual budget of
1841 dissolved inorganic carbon in the northwestern Mediterranean deep-convection region, *Biogeosciences*, 20,
1842 4683–4710, <https://doi.org/10.5194/bg-20-4683-2023>, 2023.

1843

1844 UNESCO: Intercomparison of total alkalinity and total inorganic carbon determinations in seawater. UNESCO
1845 Tech. Pap. Mar. Sci. 59., 1990

1846

1847 UNESCO: Reference materials for oceanic carbon dioxide measurements. UNESCO Tech. Pap. Mar. Sci. 60.,
1848 1991
1849
1850 United Nations. The Sustainable Development Goals 2020, 68pp. <https://unstats.un.org/sdgs/report/2020/>, 2020
1851
1852 Vance, J. M., Currie, K., Suanda, S. H. and Law, C. S.: Drivers of seasonal to decadal mixed layer carbon cycle
1853 variability in subantarctic water in the Munida Time Series. *Front. Mar. Sci.* 11:1309560. doi:
1854 10.3389/fmars.2024.1309560, 2024
1855
1856 VERNEY Romaric, RABOUILLE Christophe (2012) MERMEX-ACCESS cruise, RV Téthys II,
1857 <https://doi.org/10.17600/12450070>
1858
1859 VIVIER Frédéric, WAELBROECK Claire, MICHEL Elisabeth (2016) NEXT STEP,
1860 <https://doi.org/10.18142/338>
1861
1862 VERNEY Romaric, RABOUILLE Christophe (2012) MERMEX-ACCESS cruise, RV Téthys II,
1863 <https://doi.org/10.17600/12450070>
1864
1865 von Schuckmann, K., Minière, A., Gues, F., Cuesta-Valero, F. J., Kirchengast, G., Adusumilli, S., Straneo, F.,
1866 Ablain, M., Allan, R. P., Barker, P. M., Beltrami, H., Blazquez, A., Boyer, T., Cheng, L., Church, J.,
1867 Desbruyeres, D., Dolman, H., Domingues, C. M., García-García, A., Giglio, D., Gilson, J. E., Gorfer, M.,
1868 Haimberger, L., Hakuba, M. Z., Hendricks, S., Hosoda, S., Johnson, G. C., Killick, R., King, B., Kolodziejczyk,
1869 N., Korosov, A., Krinner, G., Kuusela, M., Landerer, F. W., Langer, M., Lavergne, T., Lawrence, I., Li, Y.,
1870 Lyman, J., Marti, F., Marzeion, B., Mayer, M., MacDougall, A. H., McDougall, T., Monselesan, D. P., Nitzbon,
1871 J., Ootosaka, I., Peng, J., Purkey, S., Roemmich, D., Sato, K., Sato, K., Savita, A., Schweiger, A., Shepherd, A.,
1872 Seneviratne, S. I., Simons, L., Slater, D. A., Slater, T., Steiner, A. K., Suga, T., Szekely, T., Thiery, W.,
1873 Timmermans, M.-L., Vanderkelen, I., Wjiffels, S. E., Wu, T., and Zemp, M.: Heat stored in the Earth system
1874 1960–2020: where does the energy go?, *Earth Syst. Sci. Data*, 15, 1675–1709, [https://doi.org/10.5194/essd-15-](https://doi.org/10.5194/essd-15-1675-2023)
1875 [1675-2023](https://doi.org/10.5194/essd-15-1675-2023), 2023.
1876
1877 Wagener, T., Metzl, N., Caffin, M., Fin, J., Helias Nunige, S., Lefevre, D., Lo Monaco, C., Rougier, G., and
1878 Moutin, T.: Carbonate system distribution, anthropogenic carbon and acidification in the western tropical South
1879 Pacific (OUTPACE 2015 transect), *Biogeosciences*, 15, 5221-5236, <https://doi.org/10.5194/bg-15-5221-2018>,
1880 2018.
1881
1882 Wimart-Rousseau, C.: Dynamiques saisonnière et pluriannuelle du système des carbonates dans les eaux de
1883 surface en mer Méditerranée, *Sciences de l'environnement*. Aix-Marseille Université, [https://hal.archives-](https://hal.archives-ouvertes.fr/tel-03523187)
1884 [ouvertes.fr/tel-03523187](https://hal.archives-ouvertes.fr/tel-03523187), 2021
1885
1886 Wimart-Rousseau, C., Lajaunie-Salla, K., Marrec, P., Wagener, T., Raimbault, P., Lagadec, V., Lafont, M.,
1887 Garcia, N., Diaz, F., Pinazo, C., Yohia, C., Garcia, F., Xueref-Remy, I., Blanc, P.-E., Armengaud, A., and
1888 Lefèvre, D.: Temporal variability of the carbonate system and air-sea CO₂ exchanges in a Mediterranean human-
1889 impacted coastal site. *Estuarine, Coastal and Shelf Science*. <https://doi.org/10.1016/j.ecss.2020.106641>, 2020.
1890
1891 Wimart-Rousseau, C., Wagener, T., Álvarez, M., Moutin, T., Fourrier, M., Coppola, L., Niclas-Chirurgien, L.,
1892 Raimbault, P., D'Ortenzio, F., Durrieu de Madron, X., Taillandier, V., Dumas, F., Conan, P., Pujo-Pay, M. and
1893 Lefèvre, D.: Seasonal and Interannual Variability of the CO₂ System in the Eastern Mediterranean Sea: A Case
1894 Study in the North Western Levantine Basin. *Front. Mar. Sci.* 8:649246. doi: 10.3389/fmars.2021.649246, 2021
1895
1896 Wimart-Rousseau, C., Wagener, T., Bosse, A., Raimbault, P., Coppola, L., Fourrier, M., Ulses, C. and Lefèvre,
1897 D.: Assessing seasonal and interannual changes in carbonate chemistry across two timeseries sites in the North
1898 Western Mediterranean Sea. *Front. Mar. Sci.* 10:1281003. doi: 10.3389/fmars.2023.1281003, 2023.
1899

1900 WMO/GCOS, 2018: <https://gcos.wmo.int/en/global-climate-indicators>, 2018
1901
1902 Yao, M. K., Marcou, O., Goyet, C., Guglielmi, V., Touratier, F., and Savy, J.-P.: Time variability of the north-
1903 western Mediterranean Sea pH over 1995-2011. Marine Environmental Research, doi:
1904 10.1016/j.marenvres.2016.02.016, 2016
1905
1906 Yoder, M. F., Palevsky, H. I., and Fogaren, K. E.: Net community production and inorganic carbon cycling in
1907 the central Irminger Sea. Journal of Geophysical Research: Oceans, 129, e2024JC021027.
1908 <https://doi.org/10.1029/2024JC021027>, 2024
1909
1910 Zhang, S., Wu, Y., Cai, W.-J., Cai, W., Feely, R. A., Wang, Z., et al. : Transport of anthropogenic carbon from
1911 the Antarctic shelf to deep Southern Ocean triggers acidification. Global Biogeochemical Cycles, 37,
1912 e2023GB007921. <https://doi.org/10.1029/2023GB007921>, 2023
1913